PHYSICAL REVIEW B VOLUME 38, NUMBER 11 15 OCTOBER 1988-I

Effect of buffer-layer composition on new optical transitions in Si/Ge short-period superlattices

M. A. Gell
British Telecommunications Research Laboratories, Martlesham Heath, Ipswich IP5 7RE, United Kingdom
(Received 20 January 1988; revised manuscript received 3 June 1988)

Local empirical pseudopotentials with spin-orbit coupling have been used to calculate transition energies and transition probabilities for the Si/Ge (4:4) superlattice grown on (001) $Si_{1-x}Ge_x$ ($0 \leq x \leq 1$) buffer layers. The characters of superlattice states close to the band edges are shown in terms of their real-space charge densities and their origin in wave-vector space. Influences of heterojunction-interface bond length and band offset are examined and the individual contributions of compositional modulation and atomic relaxation to the enhancement of matrix elements for cross-gap quasidirect transitions are established. A strain-induced reversal of $|m_J| = \frac{3}{2}$ and $|m_J| = \frac{1}{2}$ valence states is demonstrated in terms of the effects on subband energy levels and polarization-dependence of cross-gap transition probabilities. In the case of the Si/Ge (4:4) superlattice grown on Si, a direct comparison is made between theoretical results and recent electroreflectance data of Pearsall *et al.* [Phys. Rev. Lett. **58**, 729 (1987)]. Comparison is also made between the results of the present empirical-pseudopotential calculations and results of recent local-density, quasiparticle, tight-binding, and effective-mass–type calculations. Predictions are made which can be used to discriminate between different transition assignments which have been given to the same structure in the electroreflectance spectra for the (4:4) superlattice grown on (001) Si.

I. INTRODUCTION

Strained-layer $Si/Si_{1-x}Ge_x$, $Si/(A^{III}B^{V})$, and $Si/(A^{II}B^{VI})$ heterosystems are attracting considerable interest with their prospects of novel electronic and optical properties and the possibility of a viable route to a Si-based heterostructure technology. Strained-layer $Si/Si_{1-x}Ge_x$ heterostructures appear to be especially promising since it is now possible by using buffer layers to grow defect-free layers of any composition to thicknesses large enough to be of use in device structures.[1–3] Thus, there is considerable potential for substantially enhancing the existing Si-based integrated-circuit technology.

Although Si is the most technologically important electronic material, it has a severe disadvantage compared with, say, GaAs since it is an indirect semiconductor: the maximum of the valence band is at the Brillouin-zone center (point Γ), while the minimum of the conduction band is near the Brillouin-zone edge (point X), as shown in Fig. 1(a). Thus, for example, the quantum efficiency of Si photodetectors for wavelengths longer than 1 μm is rather poor.[4] However, by constructing heteroepitaxial structures of Si and Ge, which is also indirect [see Fig. 1(b)], it may be possible to create new artificial crystals with quasidirect character. This important problem was first addressed theoretically as long ago as 1974 by Gnutzmann and Clausecker,[5] although the aspect of strain resulting from the 4% lattice mismatch between Si and Ge was not incorporated within their calculations. The effect of the lattice mismatch was also neglected in the model calculations of Jackson and People.[6] However, consideration of the effects of strain on band structure have been shown to be crucial in unravelling otherwise apparently conflicting experimental measurements.[7–10] More recently, strain-induced confinement has been demonstrated clearly in the calculations of Morrison *et al.*[11,12] In that work it was also shown that interesting momentum-mixing effects leading to enhanced optical matrix elements for transitions across the zone-center gap may be expected in short-period $Si/Si_{0.5}Ge_{0.5}$ (001) superlattices grown on $Si_{0.75}Ge_{0.25}$ buffer layers. Effects of disorder scattering, studied using the coherent-potential approximation, have been discussed by Ting and Chang.[13],

Turning to the experimental side, Pearsall *et al.*, have recently presented electroreflectance data on short-period Si/Ge (001) superlattices grown on (001) Si substrates.[14] It is clear from the electroreflectance spectra that structure exists which more than likely originates from the Si/Ge superlattices. Recently, the origin of this structure, particularly for the case of the Si/Ge (4:4) superlattice[15] has been investigated using local-density (and quasiparticle),[16] effective-mass–type,[17] and tight-binding[18] calculations. In this paper we present results of calculations based on empirical local pseudopotentials with spin-orbit coupling which demonstrate that the basic conjectures of Pearsall *et al.*[14] concerning the Si/Ge (4:4) superlattice are correct. Comparison is also made between the results of the present empirical pseudopotential calculations and results of the other recent calculations and predictions are made which can be used to discriminate between different transition assignments which have been given to the same structure in the electroreflectance spectra for the (4:4) superlattice grown on (001) Si.

 ©1988 The American Physical Society

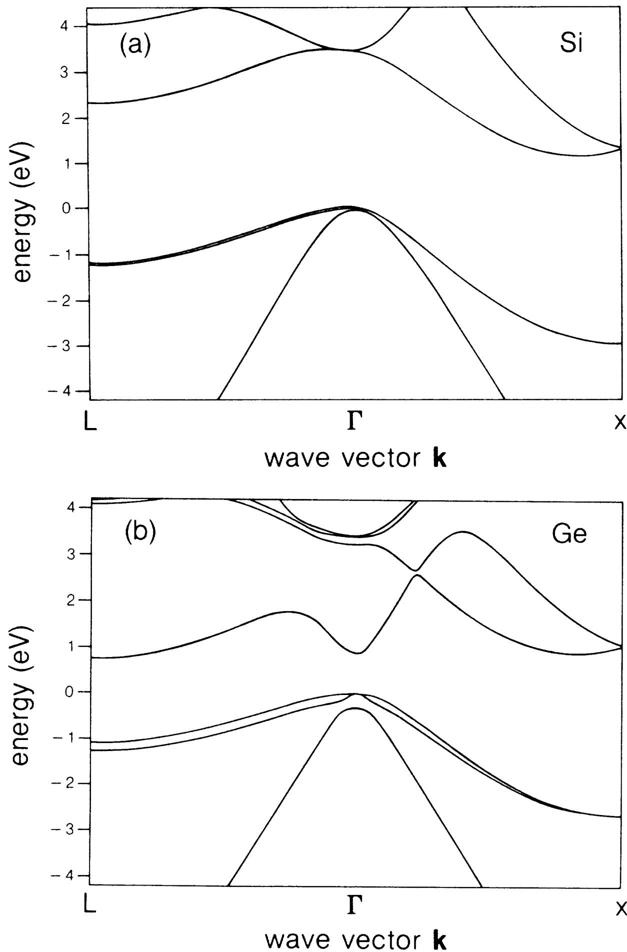

FIG. 1. Band structure of (a) Si and (b) Ge along the lines Δ and Λ, calculated using local pseudopotentials with spin-orbit coupling. The zero of energy has been taken to be the top of the valence band at Γ.

II. METHOD

The calculations are based on an extension of a method using empirical pseudopotentials, which has been used successfully to calculate electronic and optical properties of various superlattices[11,12,19–23] and, more recently, quantum wires.[24] In particular, zone-folding phenomena in short-period GaAs/AlAs superlattices have been predicted[20] in good agreement with experiment.[25] The reader is referred to these various works for background to the calculations.

The local form factors for bulk Si and bulk Ge used in the present calculations have been adjusted so as to reproduce experimentally determined transition energies as well as possible, bearing in mind the effects of nonlocality.[26–29] The nonzero form factors, as permitted by symmetry,[30] are -0.112, 0.025, and 0.041 a.u. for Si and -0.117, 0.004 25, and 0.0285 a.u. for Ge. The strained crystal is viewed as a new crystal with a different Bravais lattice, which is used to determine the new reciprocal lattice. Most of the contribution to the spin-orbit matrix elements comes from the regions of space close to the atomic sites where the potential is rapidly varying. Since these core regions are fairly incompressible, it is assumed that the spin-orbit constants λ (Ref. 29) in the small-k approximation[31] are independent of strain. The lattice constants which we used in the calculations are $A_{\mathrm{Si}}=5.431$ Å and $A_{\mathrm{Ge}}=5.657$ Å. Where necessary, the virtual-crystal approximation is used to model the alloy. In Tables I and II, values of energy levels calculated at principal symmetry points and at the minimum along Δ are given for cubic Si and cubic Ge. Corresponding values taken from the nonlocal empirical pseudopotential band structures of Chelikowsky and Cohen[29] are shown for comparison together with values given by Van de Walle and Martin[32] and various low-temperature ($\sim$0 K) transition energies determined from experiment.

Effects of lattice mismatch on strain accommodation within heteroepitaxial structures have been discussed by several authors.[32,36–41] For the case of a Si/Ge superlattice with layers consisting of a few monolayers, grown commensurately on (001) Si, the in-plane lattice constants $A_{\mathrm{Si},xy}$ and $A_{\mathrm{Ge},xy}$ of the Si and Ge layers are, to a good

TABLE I. Eigenvalues for cubic Si at Γ, X, L, and at the minimum along Δ. Comparison is made with selected values from the nonlocal empirical pseudopotential band structure of Chelikowsky and Cohen (Ref. 29) and the local-density band structure of Van de Walle and Martin (Ref. 32), and with experimental transition energies. All energies are in eV.

Point	Level	Theory	Expt.
Γ	Γ_6^v	-12.58	
		-12.36^a	
	Γ_7^v	0.044	
	Γ_8^v	0.00	
	Γ_7^c	4.42	4.19 ± 0.01^b
		4.10^a	
	Γ_6^c	3.51	3.37 ± 0.03^b
	Γ_8^c	3.53	
		3.43^a	
		2.55^c	
X	X_5^v	-2.94	
		-2.86^a	
	X_5^c	1.31	
		1.17^a	
		0.64^c	
Δ	Δ	1.17	1.17^b
L	$L_{4,5}^v$	-1.22	
		-1.23^a	
	L_6^c	2.28	2.06 ± 0.03^d
		2.23^a	
		1.45^c	
	L_6^c	4.12	
		4.34^a	
	$L_{4,5}^c$	4.13	

[a]Reference 29.
[b]Reference 33.
[c]Reference 32.
[d]Reference 34.

TABLE II. Eigenvalues for cubic Ge at Γ, X, L, and at the minimum along Δ. Comparison is made with selected values from the nonlocal empirical pseudopotential band structure of Chelikowsky and Cohen (Ref. 29) and the local-density band structure of Van de Walle and Martin (Ref. 32), and with experimental transition energies. All energies are in eV.

Point	Level	Theory	Expt.
Γ	Γ_6^v	−12.20	
		−12.66[a]	
	Γ_7^v	−0.30	0.29[b]
		−0.29[a]	
	Γ_8^v	0.00	
	Γ_7^c	0.86	0.89[b]
		0.90[a]	
		0.02[c]	
	Γ_6^c	3.23	3.00[b]
		3.01[a]	
	Γ_8^c	3.43	
		3.22[a]	
X	X_5^v	−2.66	
		−3.29[a]	
	X_5^c	1.05	
		1.16[a]	
		0.61[c]	
Δ	Δ	0.90	
L	$L_{4,5}^v$	−1.09	
		−1.43[a]	
	L_6^c	0.75	0.74[b]
		0.76[a]	
		0.09[c]	
	L_6^c	4.08	
		4.16[a]	
	$L_{4,5}^c$	4.16	
		4.25[a]	

[a]Reference 29.
[b]Reference 35.
[c]Reference 32.

approximation, expected to be determined by the lattice constant of the substrate; thus, $A_{\mathrm{Si},xy}=A_{\mathrm{Si}}$ and $A_{\mathrm{Ge},xy}=A_{\mathrm{Si}}$. The lattice spacings along the superlattice axis are, to a good approximation,[32] determined from considerations of the elastic response of the individual bulk crystals. Thus $A_{\mathrm{Si},z}=A_{\mathrm{Si}}$ and $A_{\mathrm{Ge},z}>A_{\mathrm{Ge}}>A_{\mathrm{Ge},xy}$; in fact, using the elastic constants given by Brantley,[42] we find $A_{\mathrm{Ge},z}=5.825$ Å. Feldman *et al.* have recently reported results of ion-channeling experiments on ultrathin epitaxial films of Ge embedded in Si which generally support an approach based on macroscopic arguments.[43]

For the purposes of the present calculations, the interatomic spacing d_{int} at the heterointerfaces is taken to be the mean of the lattice spacings of the constituent (unstrained) materials of the superlattice, i.e., $d_{\mathrm{int}}=\frac{1}{8}(A_{\mathrm{Si}}+A_{\mathrm{Ge}})$. However, in order to check the sensitivity of the results to this choice, calculations have also been performed with $d_{\mathrm{int}}=A_{\mathrm{Si}}/4$ and $d_{\mathrm{int}}=A_{\mathrm{Ge}}/4$; this point will be discussed later.

III. BULK Si AND Ge

The effect of uniaxial stress on a crystal is to lower the symmetry of the lattice[44] and so produce splittings of otherwise degenerate states and modify optical selection rules.[45,46] Such effects have been investigated in great detail by optical piezoabsorption, piezoreflectance, and various other measurements; the reader is referred to the review papers by Keyes[47] and Pollak.[48] In order to illustrate the effects of uniaxial stress, the band structures along $\Delta_{x,y}$ and Δ_z of tetragonal Si on (001) cubic Ge and tetragonal Ge on (001) cubic Si are shown in Fig. 2; specific energy levels are shown schematically in Figs. 3 and 4. By comparing Fig. 1 with Fig. 2, it can be seen that splittings have occurred at the important zone-center (Γ) and zone-edge (X) regions. Since the Γ_7^c level

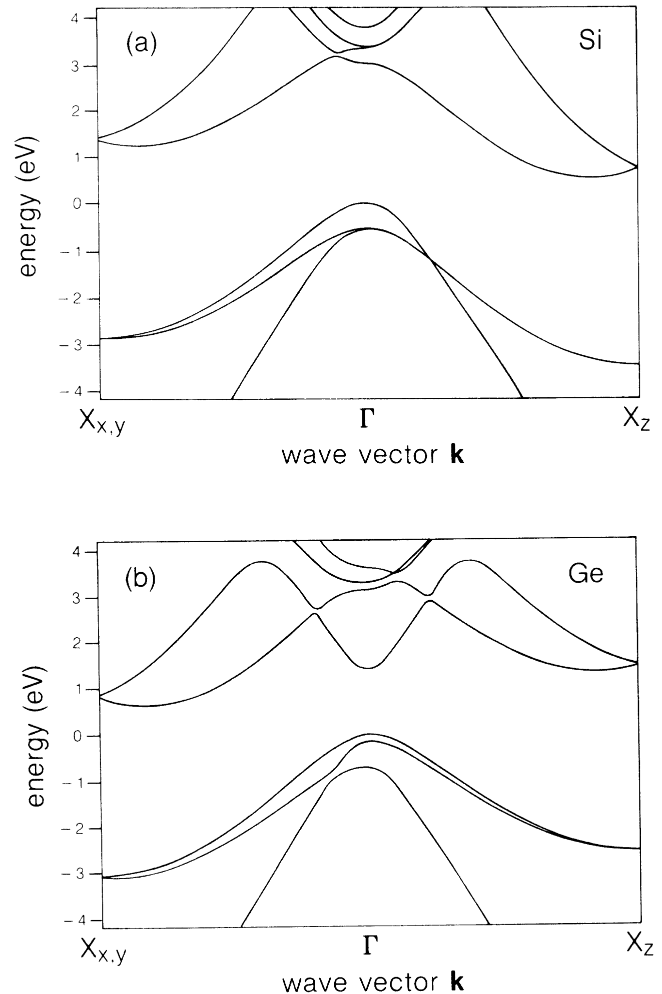

FIG. 2. Band structure of (a) tetragonal Si [on (001) cubic Ge] and (b) tetragonal Ge [on (001) cubic Si] along the Δ lines. The left-hand side of each panel shows the band structure between Γ and $X_{x,y}$ and the right-hand side shows the band structure between Γ and X_z. The zero of energy has been taken to be the top of the valence band at Γ. These band structures should be compared with the sections of band structure given on the *right*-hand side of Figs. 1(a) and 1(b).

has full cubic symmetry, it is affected only by the hydrostatic component of the strain. The main effect of the hydrostatic component is the transfer of charge away from the atomic and bond sites to the antibonding region or to other regions away from the atomic and bond sites. The [001] strain does not distinguish between L valleys.

At the center of the zone for the case of tetragonal Si on (001) cubic Ge, the effect of the compressive strain in the [001] direction is a decrease in the overlap between the p_z orbitals on neighboring atoms and an increase in the overlap between p_x and p_y orbitals. This has the effect of weakening the p_z bond and strengthening the p_x, p_y bonds. Thus, in the absence of spin-orbit coupling, the p_z (light-hole) state moves up in energy and the p_x, p_y (heavy-hole) states move down in energy. There is substantial mixing of the $|\frac{3}{2}, \pm\frac{1}{2}\rangle$ and $|\frac{1}{2}, \pm\frac{1}{2}\rangle$ bands, leading to a repulsion of the levels. Similar but opposite effects occur in the case of tetragonal Ge on (001) cubic Si.[49–55] These shifts result in substantial anisotropy in the effective masses at Γ. As far as the lowest conduction bands are concerned,[53] it can be seen from Fig. 3 that, for tetragonal Si on (001) cubic Ge, the conduction-band

TABLE III. Theoretical and experimental values for the valence-band deformation potential b and the Δ conduction-band deformation potential constant Ξ_Δ^u in Si and Ge. The deformation potentials calculated here correspond to values (in eV) obtained with tetragonal Si on (001) cubic Ge and tetragonal Ge on (001) cubic Si. The values of b have been calculated with the spin-orbit splittings switched off.

	Si	Ge
b	-2.38^d	-2.74^d
	-2.35^a	-2.55^a
	-2.19^b	-3.1^b
	-2.10 ± 0.10^c	-2.86 ± 0.15^e
Ξ_Δ^u	9.73^d	9.50^d
	9.16^a	9.42^a
	3.37^b	4.37^b
	8.6 ± 0.4^c	

[a]Reference 32.
[b]Reference 18.
[c]Reference 54.
[d]This work.
[e]Reference 55.

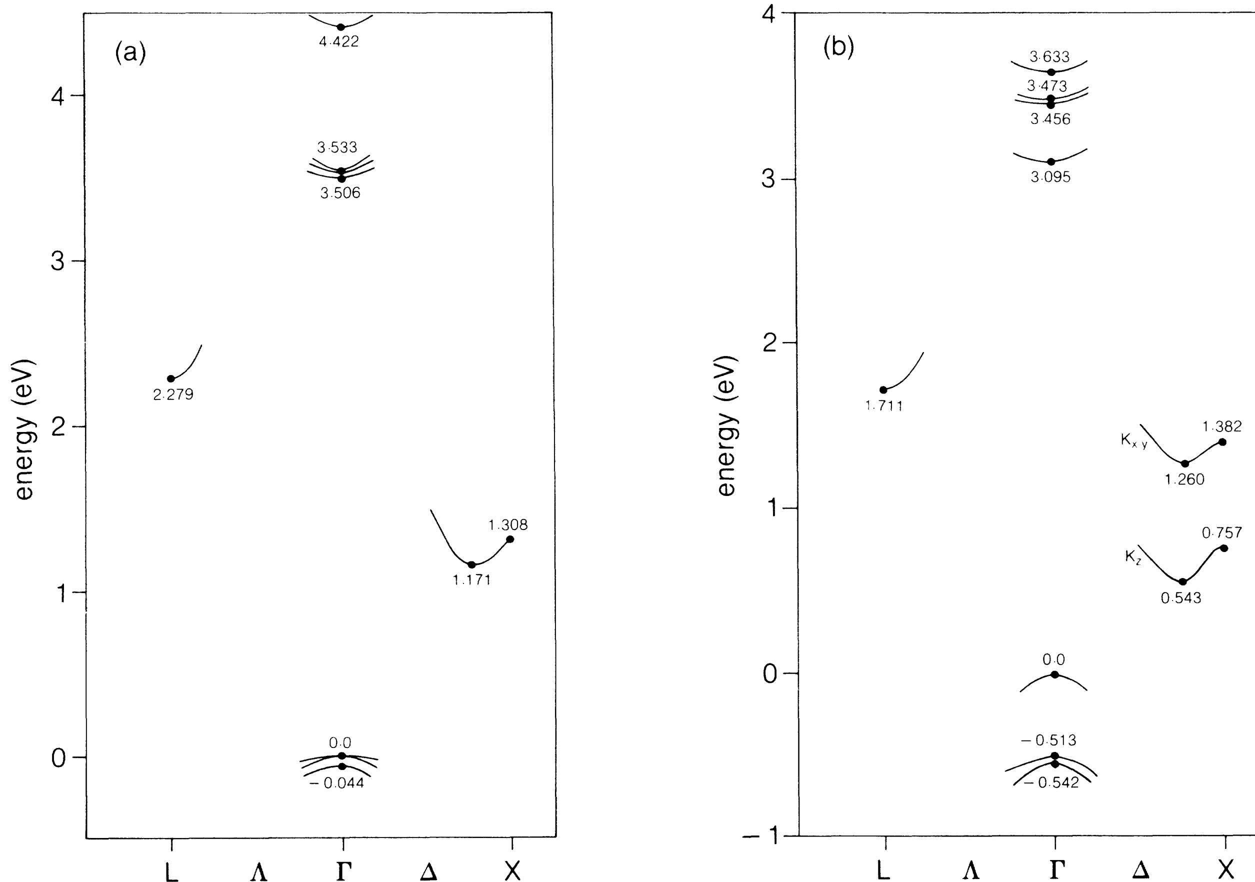

FIG. 3. Energy levels of (a) cubic Si and (b) tetragonal Si [on (001) cubic Ge] at high-symmetry points. The camel's-back structure along Δ is also illustrated.

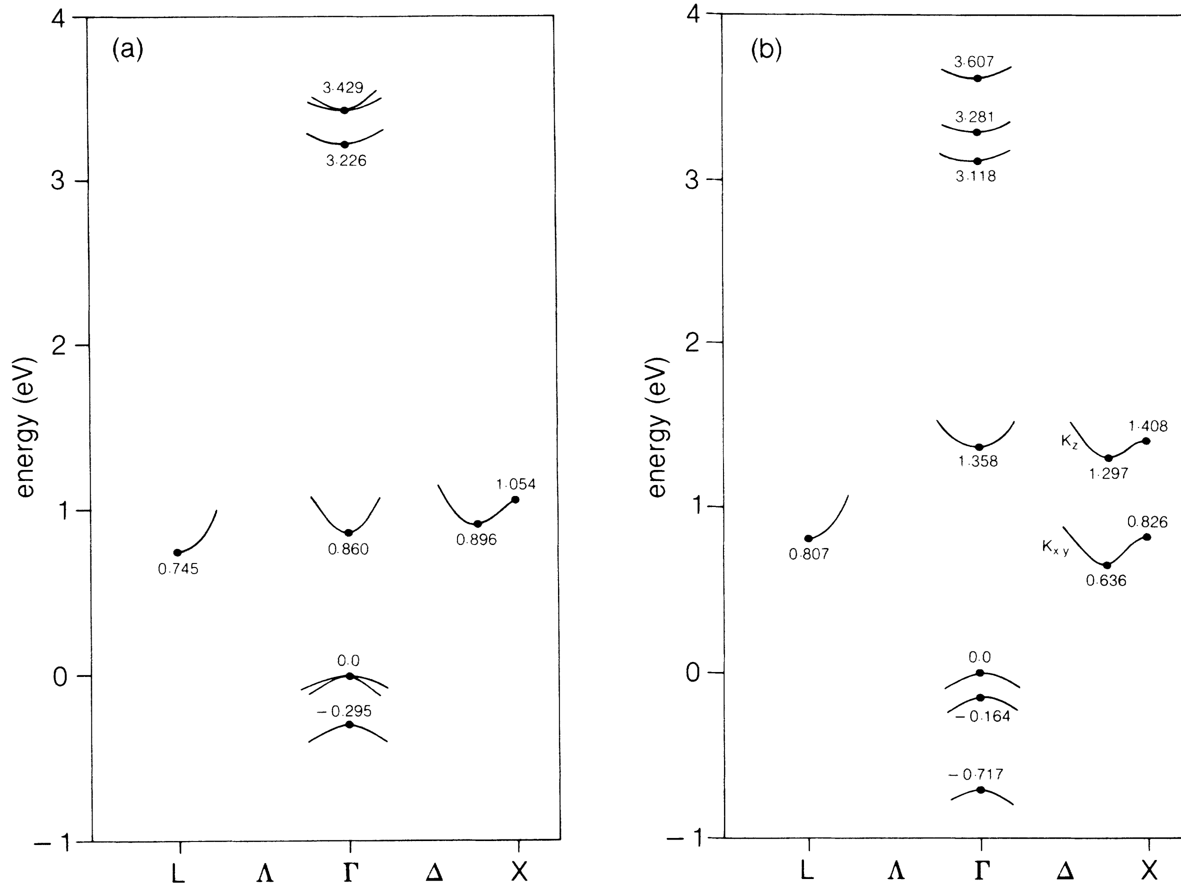

FIG. 4. Energy levels of (a) cubic Ge and (b) tetragonal Ge [on (001) cubic Si] at high-symmetry points. The camel's-back structure along Δ is also illustrated.

minima lying along [100], [$\bar{1}$00], [010], and [0$\bar{1}$0] are split off and pushed up with respect to those lying in the [001] and [00$\bar{1}$] directions. The movement of the two sets of valleys is reversed for the case of tetragonal Ge on (001) cubic Si, which becomes indirect on account of the Δ_{xy} minima rather than the L minima (see Fig. 4). The depth of the "camel's back" is increased in the case of those Δ minima which are lowered in energy. There is no camel's-back structure associated with the L valleys. Deformation potentials calculated for these structures are given in Table III; comparison is made with other values available in the literature.

IV. Si/Ge (4:4) SUPERLATTICE ON (001) Si: THEORY

In Fig. 5(a) we show the energy levels calculated at the center of the superlattice Brillouin zone (SBZ) for the top three valence states and the lowest five conduction states in the Si/Ge (4:4) superlattice grown on (001) Si. The states are labeled either as valence Vi or conduction Ci states with integer $i=1,2,3,\ldots$ such that a state closest to the band edge is assigned $i=1$. Unless otherwise stated, all of the results presented in this paper have been obtained from calculations using the offsets given by Van de Walle and Martin.[32] A wealth of states exists both above and below those illustrated in Fig. 5. In particular, the states lying immediately above state $C5$ are associated with the bulk zone-center antibonding complexes. Charge densities for these eight states are shown in Fig. 6. These charge densities have been calculated in an x-z plane which passes through atomic positions. It can be seen from Fig. 6 that the lowest two conduction-band states $C1$ and $C2$ are fairly well confined in the Si layers, although state $C2$ does have some zone-center admixture resulting in s-type charge-density components in the Ge layers. The complementary nature of the charge densities of these two states is similar to that of the charge densities of the two corresponding states in the Si/Ge (6:6) superlattice shown by Froyen *et al.*[16] State $C3$ is distributed throughout both the Si and Ge layers, while state $C4$ is reminiscent of the resonant zone-edge-related states which are found in other structures such as $GaAs/Al_xGa_{1-x}As$ (001) superlattices.[23] State $C5$ is clearly rather different from the lower conduction-band states. It originates predominantly from the zone-center region of Ge and so its charge density, localized mostly in the Ge layers, is concentrated around the atomic sites: the state is predominantly s-like. This is in contrast with states associated with the zone edge of Si and Ge bulk crystals, which have a significant amount of p and d character in their wave functions and so are rather delocal-

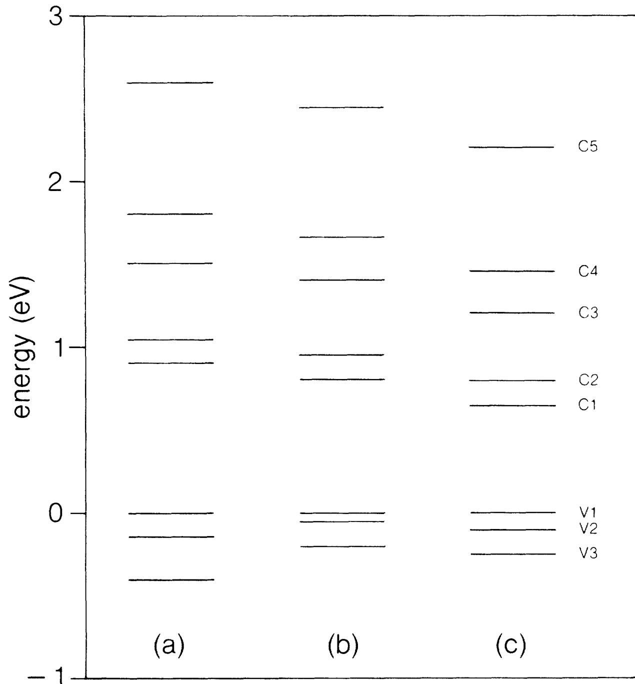

FIG. 5. Energy levels of the top three valence states ($V1-V3$) and the bottom five conduction states ($C1-C5$) at the center of the superlattice Brillouin zone in the Si/Ge (4:4) (001) superlattice. The three cases correspond to different (001) buffer layers: (a) Si, (b) $Si_{0.5}Ge_{0.5}$, and (c) Ge. In each case the zero of energy has been taken as the energy of the top valence state, $V1$. Conduction states $C1-C4$ are zone-edge-related states, while state $C5$ is the ground zone-center-related state (see Table IV).

ized or free-electron-like throughout the bulk-crystal unit cell.[56] The mechanism of orthogonalization of interacting zone-center and zone-edge-related states is similar to that which has been shown to exist in GaAs/AlGaAs superlattices;[23] this mechanism is essentially independent of the distribution of strain within the unit cell. The momentum-mixing effects, controlled by the phases of the states, give rise to enhanced cross-gap transition probabilities.

In order to provide further insight into the superlattice states shown in Fig. 6, the spectral distributions (cf. Ref. 20) of the states are shown in Table IV. It can be seen from Table IV, for example, that state $C5$ is constructed mostly from the lowest two conduction bands of the host crystal (tetragonal $Si_{0.5}Ge_{0.5}$). There is coupling to the coupled[48] $|m_J|=\frac{1}{2}$ bands (bands 2 and 3) and to higher conduction bands (not shown) and there is significant momentum mixing across the host-crystal Brillouin zone; there is no coupling to the $|m_J|=\frac{3}{2}$ band (band 4). The full charge density is not purely s-like, but is complicated by the introduction of sp components into its wave function. sp_z hybridization, concomitant with a shift in charge density away from the atomic sites, is especially evident in the Si region. The spectral distributions in Table IV show that the lowest four conduction-band states (states $C1-C4$) are derived essentially from host-crystal conduction-band states belonging predominantly to the outer half of the host-crystal Brillouin zone.

The spectral distributions of states $V1-V3$ show that the uppermost valence-band states are derived from a rather restricted region of wave-vector space centered on Γ. Bearing in mind that the host crystal states at the top of valence band correspond to strain-split states (the energy separation of bands 3 and 4 at the zone center of the strained host crystal is about 0.1 eV), it is clear from inspection of the spectral distributions of the superlattice valence-band states in Table IV that significant heavy-hole–light-hole mixing is occurring. There is also coupling between the valence and conduction bands, especially in the split-off state $V3$.

V. COMPARISON WITH EXPERIMENT

In order to make a comparison between the results of the present theory and the results presented by Pearsall *et al.*,[14] values of $\log_{10}$ of the modulus squared of the optical matrix elements for all transitions between the valence- ($V1-V3$) and conduction-band ($C1-C5$) states of Fig. 5(a) have been plotted against transition energy in the lower part of Fig. 7(a). The present calculations do not include excitonic effects. The matrix elements used to construct Fig. 7(a) have been calculated with the polarization vector lying in the plane of the heterointerface. Corresponding matrix elements calculated for light polarized along the superlattice axis are plotted in Fig. 7(b). Room-temperature electroreflectance data[14] for a (4:4) superlattice on (001) Si are shown in the upper part of Fig. 7(a). The theoretical transition energies, based on 0-K bulk band structures, have been reduced by 0.1 eV in order to facilitate comparison with the electroreflectance data.

Critical points, necessarily present at points of high symmetry in the Brillouin zone, introduce structure in the joint-density-of-states function, which, in turn, gives rise to structure in the electroreflectance spectrum. In fact, it can be seen that there is reasonable correlation between features in the electroreflectance spectra and the theoretical predictions for zone-center transitions. In particular, both the theoretical and the experimental spectra are rich in structure below 1.6 eV, which cannot arise from an equivalent alloy structure. However, it is not yet entirely clear how the room-temperature electroreflectance spectra should be interpreted, especially in connection with line-shape analysis, the shortness of the superlattices (breakdown of k_z as a good quantum number), and complications associated with atomic terracing and phonon assistance of transitions. Fluctuations in the widths of the superlattice layers will readily produce fluctuations of the superlattice transition energies by one- or two-tenths of an eV. For example, additional biatomic steps in some of the Si layers would give rise to reductions in the lowest zone-center transition energies by about 0.1–0.2 eV, since the lowest conduction-band states are well confined in the Si layers. Much more information (e.g., on superlattice length, temperature, polarization, electric field, and phase dependence of the electroreflectance spectra) is required for a more complete identification of critical points.

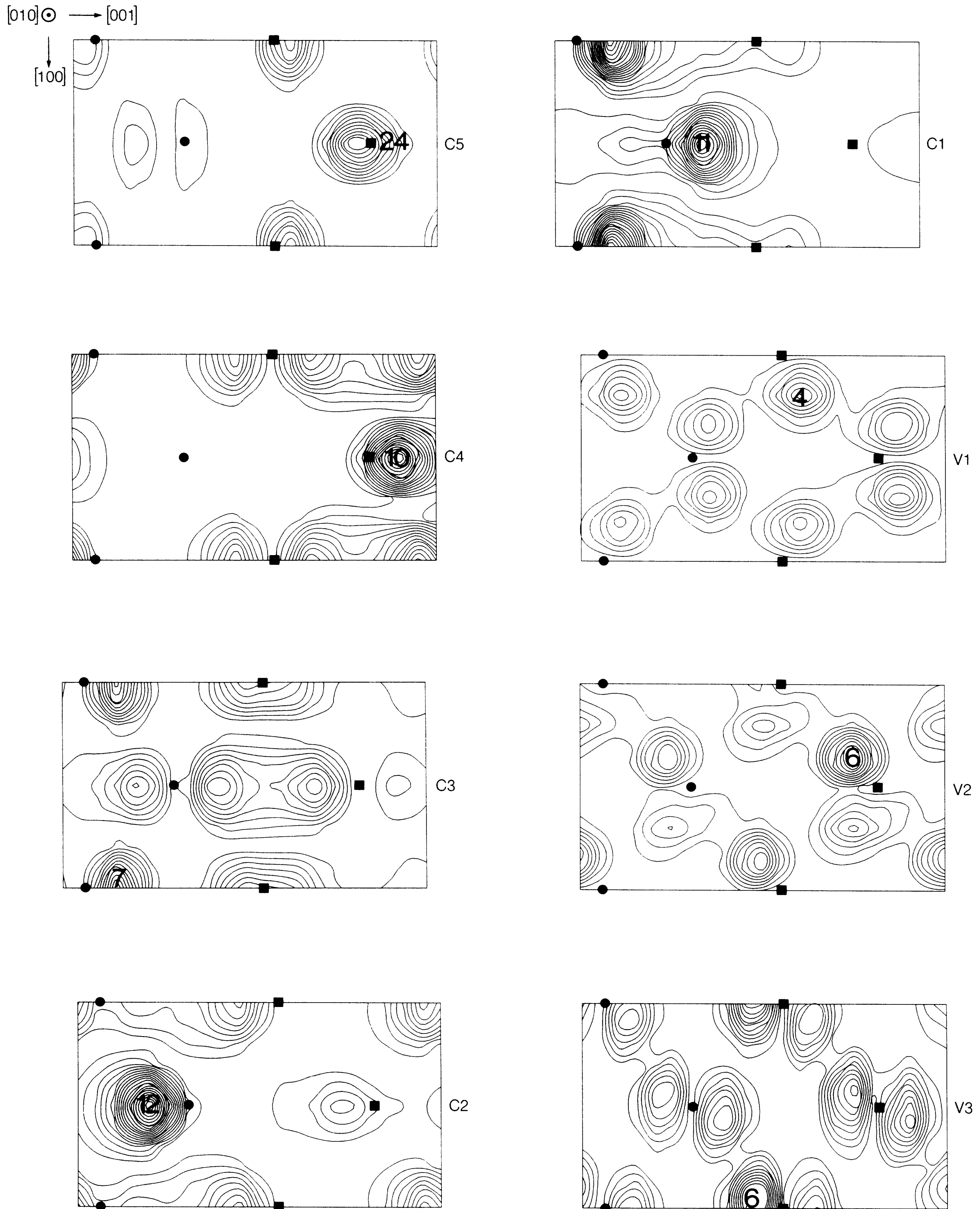

FIG. 6. Charge-density contour plots of the eight states $V3-C5$ shown in Fig. 5(a). The charge densities have been plotted (with $V3-C4$ contour spacings of 0.5 a.u. and $C5$ contour spacings of 2.0 a.u.) in an x-z plane which passes through atomic sites, marked ● (Si) and ■ (Ge). The numbers indicate the peak charge densities.

Bearing in mind that the layers are only about 5–6 Å in thickness, it is not surprising that the observed transitions are fairly broad, although electroreflectance often gives rise to broad features in regions with several transitions. The large number of transitions in the range 1.2–1.6 eV account for the broadening on the high-energy side of the feature observed around 1.2 eV. However, it would appear that there is some discrepancy in the assignment of transitions to the features observed between 2.3 and 3.0 eV. In the present work there are no allowed transitions at the center of the SBZ which account for the strong feature at 2.3 eV. The implication of the present work is that this structure originates from a critical point(s) away from the zone center. In fact, several dipole-allowed transitions at 0 K are predicted to occur around 2.4 and 2.8 eV (and at higher energies). These transitions originate from distinct points in the SBZ associated with mappings of the host-crystal L valleys. This contrasts with the results of calculations, apart from the local-density calculations, described in Refs. 16–18, which indicate that structure at 2.3 eV at 300 K is also connected with transitions at Γ from the top of the

TABLE IV. Sum over spin of the moduli squared of the leading coefficients in the expansion of the states shown in Fig. 5(a) at the center of the superlattice Brillouin zone in the Si/Ge (4:4) superlattice on (001) cubic Si. The wave vectors are in units of 2π/(lattice constant of the unstrained host crystal). For each superlattice state, the coefficients, normalized so that the largest coefficient is 1, are shown separately for the four valence bands (bands 1–4, with band index increasing with increasing energy) and for the lowest four conduction bands (bands 5–8).

Band	Wave vector k_z −1.0	−0.5	0.0	0.5	Band	Wave vector k_z −1.0	−0.5	0.0	0.5
		State $C5$					State $C1$		
8	0.0000	0.0000	0.0220	0.0000	8	0.0000	0.0000	0.0000	0.0000
7	0.0000	0.0001	0.0000	0.0001	7	0.0000	0.0000	0.0000	0.0000
6	0.0013	0.1977	0.0034	0.1993	6	0.6173	0.0070	0.0000	0.0104
5	0.0011	0.0186	1.0000	0.0189	5	1.0000	0.2592	0.0002	0.2031
4	0.0000	0.0000	0.0000	0.0000	4	0.0000	0.0000	0.0000	0.0000
3	0.0000	0.0000	0.0018	0.0000	3	0.0000	0.0000	0.0019	0.0000
2	0.0006	0.0085	0.0106	0.0084	2	0.0011	0.0019	0.0119	0.0014
1	0.0006	0.0004	0.0000	0.0004	1	0.0018	0.0013	0.0008	0.0007
		State $C4$					State $V1$		
8	0.0000	0.0000	0.0000	0.0000	8	0.0000	0.0004	0.0004	0.0004
7	0.0000	0.0000	0.0000	0.0000	7	0.0000	0.0007	0.0015	0.0007
6	0.2985	0.0053	0.0000	0.0044	6	0.0000	0.0001	0.0075	0.0001
5	0.2687	1.0000	0.0002	0.9959	5	0.0000	0.0000	0.0001	0.0000
4	0.0000	0.0000	0.0000	0.0000	4	0.0001	0.0038	1.0000	0.0038
3	0.0000	0.0000	0.0015	0.0000	3	0.0001	0.0006	0.2115	0.0006
2	0.0006	0.0005	0.0107	0.0005	2	0.0000	0.0000	0.0047	0.0000
1	0.0005	0.0012	0.0042	0.0012	1	0.0000	0.0000	0.0000	0.0000
		State $C3$					State $V2$		
8	0.0000	0.0000	0.1426	0.0000	8	0.0000	0.0004	0.0001	0.0004
7	0.0000	0.0000	0.0000	0.0000	7	0.0000	0.0000	0.0064	0.0000
6	0.1010	0.0097	0.0088	0.0096	6	0.0002	0.0009	0.0016	0.0009
5	0.0990	1.0000	0.0669	0.9813	5	0.0002	0.0006	0.0014	0.0006
4	0.0000	0.0000	0.0000	0.0000	4	0.0006	0.0012	0.2127	0.0012
3	0.0000	0.0000	0.0001	0.0000	3	0.0006	0.0032	1.0000	0.0032
2	0.0005	0.0026	0.0005	0.0027	2	0.0000	0.0002	0.0004	0.0002
1	0.0004	0.0016	0.0001	0.0016	1	0.0000	0.0000	0.0000	0.0000
		State $C2$					State $V3$		
8	0.0000	0.0000	0.0029	0.0000	8	0.0000	0.0001	0.0000	0.0001
7	0.0000	0.0000	0.0000	0.0000	7	0.0000	0.0000	0.0007	0.0000
6	1.0000	0.0098	0.0002	0.0064	6	0.0012	0.0073	0.0000	0.0073
5	0.6850	0.0482	0.0071	0.1152	5	0.0013	0.0043	0.0101	0.0043
4	0.0000	0.0000	0.0000	0.0000	4	0.0000	0.0001	0.0024	0.0001
3	0.0000	0.0000	0.0000	0.0000	3	0.0000	0.0001	0.0011	0.0001
2	0.0020	0.0001	0.0002	0.0004	2	0.0003	0.0010	1.0000	0.0010
1	0.0014	0.0017	0.0000	0.0023	1	0.0003	0.0000	0.0001	0.0000

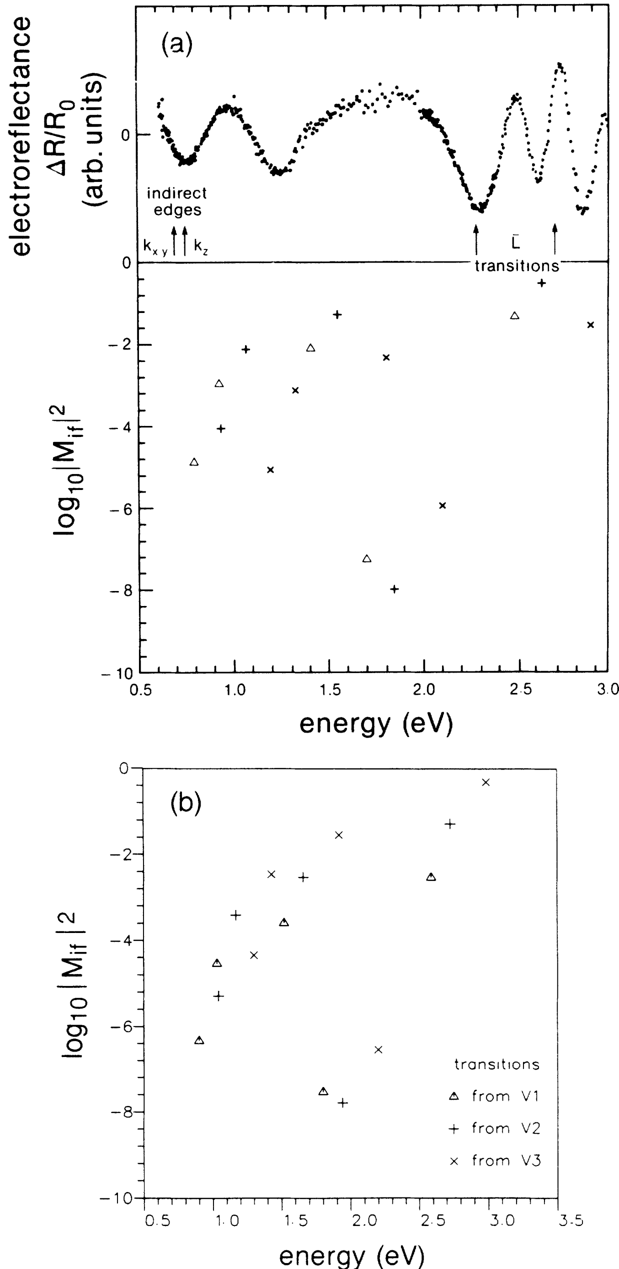

FIG. 7. (a) *Lower part*: Plot of $\log_{10}$ of the modulus squared of the optical dipole matrix element against transition energy for all zone-center cross-gap transitions between the valence and conduction states shown in Fig. 5(a) at $x=0$. The polarization vector has been chosen to lie in the [110] direction. The symbols $\triangle$, $+$, and $\times$ represent transitions from states $V1$, $V2$, and $V3$, respectively. The transition energies have been reduced by 0.1 eV compared with the calculated values in order to facilitate comparison with experiment. Corrections to energy levels for the shortness of the superlattice embedded within Si are of the order of the convergence error within the calculation (see Sec. VI). *Upper part*: Room-temperature electroreflectance data of Pearsall *et al.* (Ref. 14) for a (4:4) superlattice on (001) Si. Theoretical values for indirect edges (along $k_{x,y}$ and k_z) and dipole-allowed transitions (denoted $\bar{L}$) associated with mapped L points are indicated. (b) Plot of $\log_{10}$ of the modulus squared of the optical dipole matrix element against transition energy for the case of [001] polarization.

valence band to state $C5$ (see Table VIII).

Within the present calculations, "in-plane" (superlattice) indirect edges are expected at 0.79 eV (heavy hole) and 0.93 eV (light hole). These values are consistent with recent photocurrent measurements (0.78 and 0.90 eV at 300 K),[16] although it is not clear whether the indirect edges, or perhaps one of the edges, observed in the experiment are those (at 0.83 and 0.97 eV) associated with the "axial" (superlattice) indirect edges or, more likely, transitions from the superlattice valence states to extended conduction states in the Si layers cladding the superlattice. These points will be discussed further in Sec. VII.

VI. Si/Ge (4:4) SUPERLATTICE ON (001) Si: THEORY CONTINUED

As mentioned earlier, the present calculations have been performed with a heterointerface bond length d_{int} taken to be one-quarter of the average of the bulk cubic lattice constants A_{Si} and A_{Ge}. In order to test the sensitivity of the results to this choice, two additional calculations have been performed with two *extreme* values of d_{int}: $d_{\text{int}}=A_{\text{Si}}/4$ and $A_{\text{Ge}}/4$. For brevity, we refer to the three different heterointerface bond-length configurations as follows:

$$\text{Case A:}\quad d_{\text{int}}=A_{\text{Si}}/4=1.358\ \text{Å}\ ,$$

$$\text{Case B:}\quad d_{\text{int}}=(A_{\text{Si}}+A_{\text{Ge}})/8=1.386\ \text{Å}\ ,$$

and

$$\text{Case C:}\quad d_{\text{int}}=A_{\text{Ge}}/4=1.414\ \text{Å}\ .$$

Energy levels calculated for the three configurations are given in Table V and corresponding logarithms of the modulus squared of the optical matrix elements with [110] and [001] polarization are presented in Table VI for the cross-gap transitions from states $V1$. It can be seen from Table V that although d_{int} changes by only 0.03 Å between cases B and A and between cases B and C, there are changes of up to ± 55 meV in some of the energy levels. The zone-center energy gaps for the three cases are 0.85 eV (A), 0.90 eV (B), and 0.93 eV (C). Examination of the spectral distributions of state $V1$ for the three cases (cases A and C not shown) shows that the ratio of the zone-center component from band 4 to that from band 3 (summing over spin states) is

Case A: 1.0:0.37 ,

Case B: 1.0:0.21 (see Table IV) ,

Case C: 1.0:0.03 .

Clearly, the degree of heavy-hole–light-hole mixing is very sensitive to the width of the heterointerface bond length and, for the structures considered here, is a minimum in case C. This is reflected, for example, in the difference between the optical matrix elements for the transition $V1$-$C5$, which shows the largest variation, i.e., 3 orders of magnitude, between [110] and [001] polariza-

TABLE V. Shown are the energy levels (in eV) calculated at the center of the superlattice Brillouin zone for the states closest to the band gap in the Si/Ge (4:4) superlattice on (001) Si. The energy levels have been calculated using three different heterointerface bond lengths: A, $d_{int}=A_{Si}/4$; B, $d_{int}=(A_{Si}+A_{Ge})/8$; C, $d_{int}=A_{Ge}/4$. In parentheses are the energy differences for the states in A and C compared with those given in B; a negative sign has been used to indicate a drop in energy with respect to the corresponding state in B. The energy levels shown in column B are plotted in Fig. 5(a). The movement of the various energy levels can be understood in terms of arguments similar to those presented in Sec. III.

State	A		B	C	
			Energy (eV)		
C5	2.646	(0.055)	2.591	2.536	(−0.055)
C4	1.749	(−0.053)	1.802	1.853	(0.051)
C3	1.490	(−0.024)	1.514	1.539	(0.025)
C2	0.982	(−0.048)	1.030	1.075	(0.045)
C1	0.875	(−0.021)	0.896	0.918	(0.022)
V1	0.022	(0.022)	0.000	−0.013	(−0.013)
V2	−0.180	(−0.037)	−0.143	−0.111	(0.032)
V3	−0.387	(0.015)	−0.402	−0.418	(−0.016)

TABLE VI. Shown is the $\log_{10}$ of the sum over spin of the modulus squared of the optical matrix elements with [110] and [001] polarizations for transitions from *V1* across the band gap at the center of the superlattice Brillouin zone in the Si/Ge (4:4) superlattice on (001) cubic Si. The three cases shown for each polarization correspond to calculations performed with three different heterointerface bond lengths (see the caption of Table V).

Initial state	Final state	[110] polarization A	[110] polarization B	[110] polarization C	[001] polarization A	[001] polarization B	[001] polarization C
V1	*C1*	−5.1	−4.9	−4.6	−6.1	−6.3	−7.1
V1	*C2*	−3.4	−3.0	−2.5	−4.6	−4.5	−5.3
V1	*C3*	−2.5	−2.1	−1.6	−3.4	−3.6	−4.4
V1	*C4*	−7.0	−7.3	−6.7	−6.9	−7.5	−8.5
V1	*C5*	−1.7	−1.3	−0.9	−2.3	−2.5	−3.7

TABLE VII. Illustrated is the convergence of $\log_{10}$ of the sum over spin of the modulus squared of the optical matrix elements with the number n of host-crystal bands (not including spin) in the expansion of the superlattice wave functions. The case with $n=8$ corresponds to the case in which the four valence bands (i.e., eight including spin) and the lowest four conduction bands are included in the basis set; increasing n corresponds to increasing the number of conduction bands. The transitions considered are transitions with [110] polarization across the band gap from state *V1* to the lowest five conduction states at the center of the superlattice Brillouin zone in the Si/Ge (4:4) superlattice on (001) cubic Si. Forbidden transitions are particularly sensitive to convergence aspects of the calculations. Indicated in parentheses are local-density (LD) results for transitions with [100] polarization as calculated by Hybertson and Schlüter (Ref. 16).

Initial state	Final state	Number of bands n: 8	12	20	40	
V1	*C5*	−1.3	−1.4	−1.3	−1.4	
V1	*C4*	−5.3	−5.4	−7.3	−8.1	
V1	*C3*	−2.1	−2.1	−2.1	−2.1	(LD: −2.2)
V1	*C2*	−3.4	−3.1	−3.0	−3.0	(LD: −3.2)
V1	*C1*	−4.7	−4.7	−4.9	−5.1	

tion in case C, compared with less than 1 order of magnitude in case A (see Table VI). Generally, however, the squared matrix elements, for a given polarization, appear to be stable to within 1 order of magnitude over the wide range of d_{int} that has been considered. Apart from shifts approaching 80 meV for some of the transitions, there are no significant changes to the picture given in Fig. 7. Uncertainties in the heterointerface bond length (and abruptness of the potential) are unlikely to affect the conclusions of this work concerning the assignment of transitions to features in the electroreflectance spectrum of Pearsall *et al.*[14] Apart from the results given in Tables V and VI, all other results in this paper correspond to case B.

For completeness, the convergence properties of the calculations are considered. The calculations are performed in *single*-precision arithmetic. In Fig. 8 the convergence of the zone-center energy levels in the (4:4) superlattice are shown as a function of the number of host-crystal bands included in the expansion set of the superlattice wave functions. It can be seen from this figure that the energy levels have substantially converged with a basis set built from 12 (i.e., 24 including spin) host-crystal bands. The most sensitive state is the *s*-like state *C*5. The fact that the energy levels converge so quickly, even though the superlattice has such a short period, stems from the fact that there is very little mixing of bands (see Table IV). The corresponding rapid convergence of the dipole matrix elements for the $V1$-Ci $(i=1-5)$ transitions is shown in Table VII. The matrix elements for the quasidirect transitions (with [100] polarization) as calculated by Hybertson and Schlüter are also shown. Bearing in mind the many differences between the two types of calculations and also the various uncertainties which exist (e.g., see Table VI), the order of magnitude agreement between the results is good. Apart from the results presented in Fig. 8 and Table VII, the results presented in this paper have been obtained using an expansion set with 20 bands. Thus, energy levels can be considered to be converged to within 20–40 meV.

VII. Si/Ge (4:4) SUPERLATTICE ON (001) $Si_{1-x}Ge_x$ $(0\le x\le 1)$

We turn our attention to two different Si/Ge (4:4) superlattices for which optical spectra are not available in the literature. We consider the case of the (4:4) superlattice grown on a $Si_{0.5}Ge_{0.5}$ buffer and on a Ge buffer. The growth direction is [001] in both cases. Macroscopic arguments, as discussed above, are used to find the atomic positions; consideration of "bond bending" is not relevant to the present configurations since the intracellular distances within each layer transform according to the macroscopic strain tensor.[57] It is assumed that the lattice constant of the buffer layer, which is playing the role of an effective substrate, is unaffected by superlattice deformation. In particular, we note that the Si and Ge layers in the superlattice on the $Si_{0.5}Ge_{0.5}$ buffer layer are symmetrically strained so that, in principle, there is no restriction on the total length of such a superlattice in the growth direction.

Energy levels for these two new superlattices are given in Figs. 5(b) and 5(b) and $\log_{10}$-squared-matrix-element–transition-energy plots are given in Figs. 9 and 10. It can be seen from Fig. 5 that there is a close correspondence between the states in the (4:4) superlattice on the three different buffer layers. The charge densities of the states for the three superlattices are fairly similar, although small changes do occur which can be traced to movement of the various band edges. The major distinction between the superlattices is the ordering of the character of the valence states (states $V1-V3$). As the Ge concentration in the buffer layer increases, the strain in

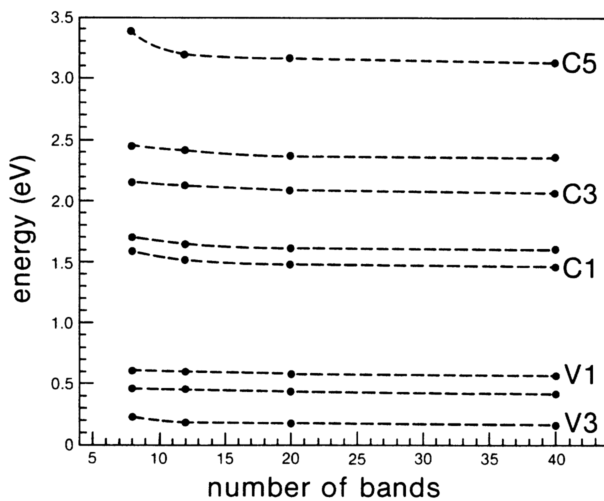

FIG. 8. Convergence of the energy levels of the states shown in Fig. 5(a) as a function of the number of host-crystal bands included in the expansion set of the superlattice wave function. The zero of energy is the top of the valence band of bulk cubic Si. The corresponding convergence of optical dipole matrix elements is shown in Table VII.

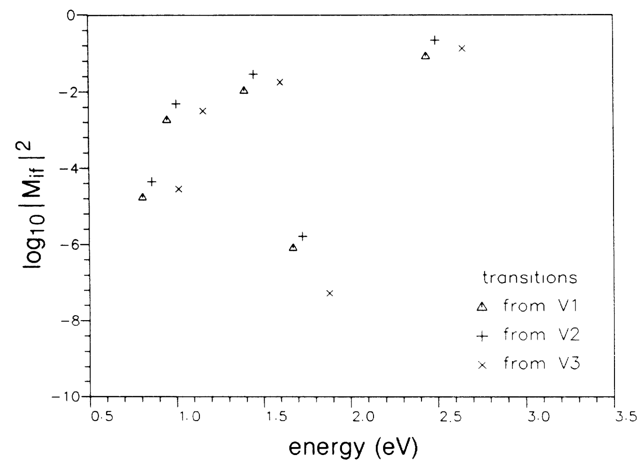

FIG. 9. Plot of $\log_{10}$ of the modulus squared of the optical matrix element against transition energy for all zone-center cross-gap transitions between the valence and conduction states shown in Fig. 5(b). The polarization vector has been chosen to lie in the [110] direction.

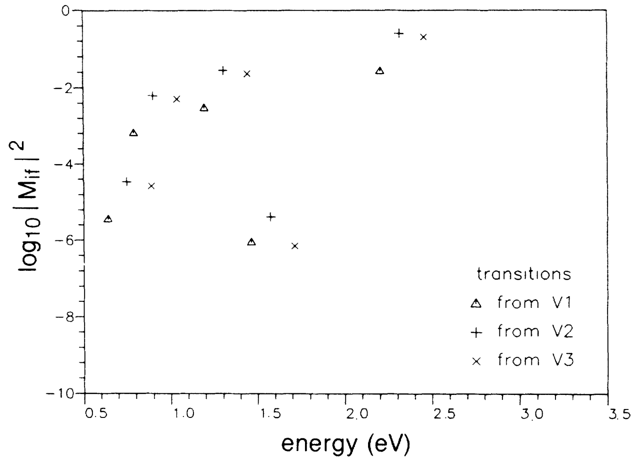

FIG. 10. Plot of $\log_{10}$ of the modulus squared of the optical matrix element against transition energy for all zone-center cross-gap transitions between the valence and conduction states shown in Fig. 5(c). The polarization vector has been chosen to lie in the [110] direction.

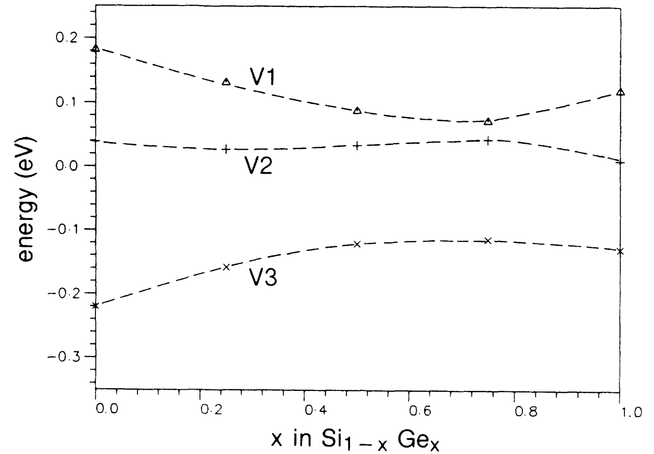

FIG. 11. Variation in energy level of the top three valence states at the center of the superlattice Brillouin zone in the Si/Ge (4:4) superlattice on (001) $Si_{1-x}Ge_x$ ($0 \leq x \leq 1$) buffer layers. The zero of energy at each buffer-layer composition has been taken as the mean energy of the three valence states. An anticrossing of the $m_J = \frac{1}{2}$ and $\frac{3}{2}$ states occurs at $x \approx 0.6$.

the Si and Ge layers changes. For the case of a Si buffer (or substrate in the case of the experiments that have been discussed) only the Ge layers are under tetragonal distortion and the top bulk Ge zone-center valence state is an $|m_J| = \frac{3}{2}$ state. For the case of a Ge buffer, only the Si layers are under tetragonal distortion and the top bulk Si zone-center valence state is an $|m_J| = \frac{1}{2}$ state. Thus, a change in the buffer-layer composition leads to substantial changes in the band structures of the constituent Si and Ge layers. For the offsets considered here, the effective heavy-hole-like barrier remains approximately constant (about 0.8 eV) for all $Si_{1-x}Ge_x$ buffers, whereas the effective light-hole-like (strictly mixed light-hole and split-off) barrier drops from about 0.7 to 0.3 eV in going from a Si to a Ge buffer. This substantial drop in the effective light-hole-like barrier, coupled with the relative positions of the zone-center bulk valence states, forces the $|m_J| = \frac{1}{2}$ zone-center superlattice state to anticross the $|m_J| = \frac{3}{2}$ state. The anticrossing can be seen very clearly in Fig. 11, in which the energies of the top three valence states have been plotted as a function of the fraction of Ge in the $Si_{1-x}Ge_x$ buffer layer. As the amount of Ge in the buffer layer is increased from 0% to 100%, the $|m_J| = \frac{3}{2}$ state shifts from being the uppermost zone-center valence state to being the state below the uppermost valence state. The crossover occurs at a Ge concentration of about 60 at. %.

The crossover also manifests itself in a change in optical properties. To illustrate this, $\log_{10}$ of the modulus squared optical matrix elements for the transitions between the top three valence states ($V1-V3$) and conduction state $C5$ have been plotted in Fig. 12 for (a) [110] and (b) [001] polarization as a function of buffer composition. It can be seen from Fig. 12(b) that the squared matrix element for the $V2$-$C5$ transition with [001] polarization drops by about 3 orders of magnitude after the crossing. This is a reflection of the decrease in p_z-like components

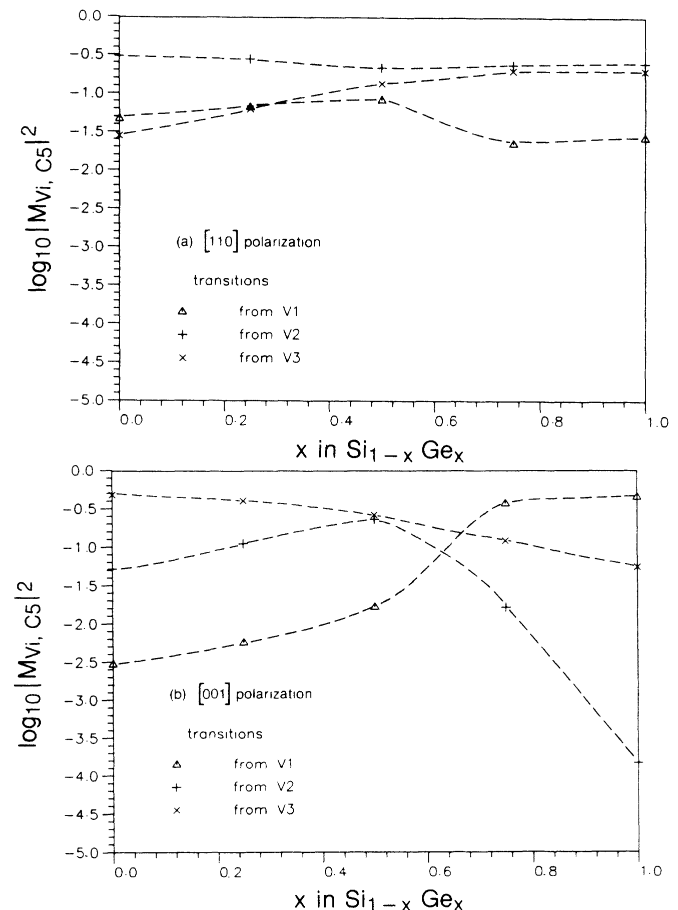

FIG. 12. Variation in $\log_{10}$ of the modulus squared optical matrix element for the zone-center cross-gap transitions between $V1$, $V2$, and $V3$ and the zone-center-related conduction state $C5$ as a function of buffer-layer composition. The polarization vector has been chosen to lie in (a) the [110] direction and (b) the [001] direction. The dashed lines are merely a guide for the eye. The energy levels of the valence states have been shown in Fig. 11.

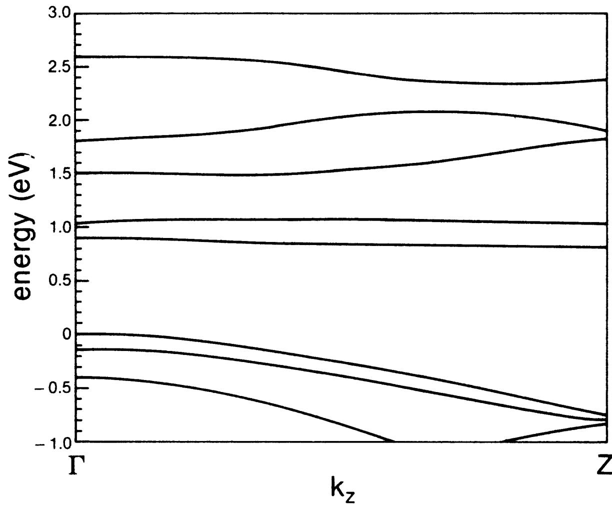

FIG. 13. Longitudinal subband dispersions of band-edge states in the Si/Ge (4:4) superlattice grown on (001) Si.

in the wave function of state $V2$ with increasing Ge concentration in the buffer layer. The corresponding drop in the value of the matrix element for the $V1$-$C5$ transition in going from [110] to [001] polarization on a Si buffer is much less, a reflection of the strong heavy-hole–light-hole mixing occurring in the superlattice. The hole reversal can also be seen directly by comparing the longitudinal subband dispersions of the Si/Ge (4:4) superlattice on (001) Si and (001) Ge; these dispersions are shown in Figs. 13 and 14, respectively. It can be seen from Fig. 14 that there is an anticrossing of the top two valence states. This anticrossing does not occur in the (4:4) superlattice on Si. It can also be seen that the dispersions of the lowest conduction states are much smaller than those of the valence-band states. This is due to the fact that the lowest conduction-band states are derived primarily from bulk zone-edge states, which are associated with large longitudinal effective mass. The anticrossings described here also occur in other Si/Ge superlattices; for a fixed period, the Ge concentration at which the hole states cross decreases as the ratio of the width of the Si layer to the width of the Ge layer increases. Similar reversals have recently been reported in absorption and gain measurements on (001)-oriented (Cd,Mn)Te and (Zn,Mn)Te strained-layer multiquantum-well structures.[58] Hole reversal has also been demonstrated in $In_xGa_{1-x}As/In_yAl_{1-y}As$ (Ref. 59) and $In_xGa_{1-x}As/InP$ (Ref. 60) strained-layer superlattices.

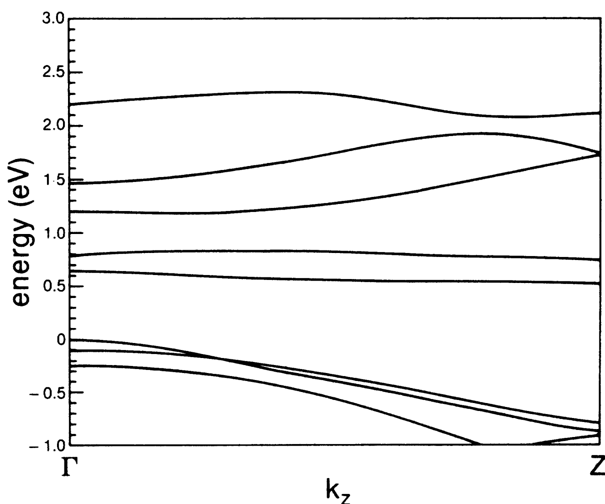

FIG. 14. Longitudinal subband dispersions of band-edge states in the Si/Ge (4:4) superlattice grown on (001) Ge.

The drop in the zone-center energy gap in going from

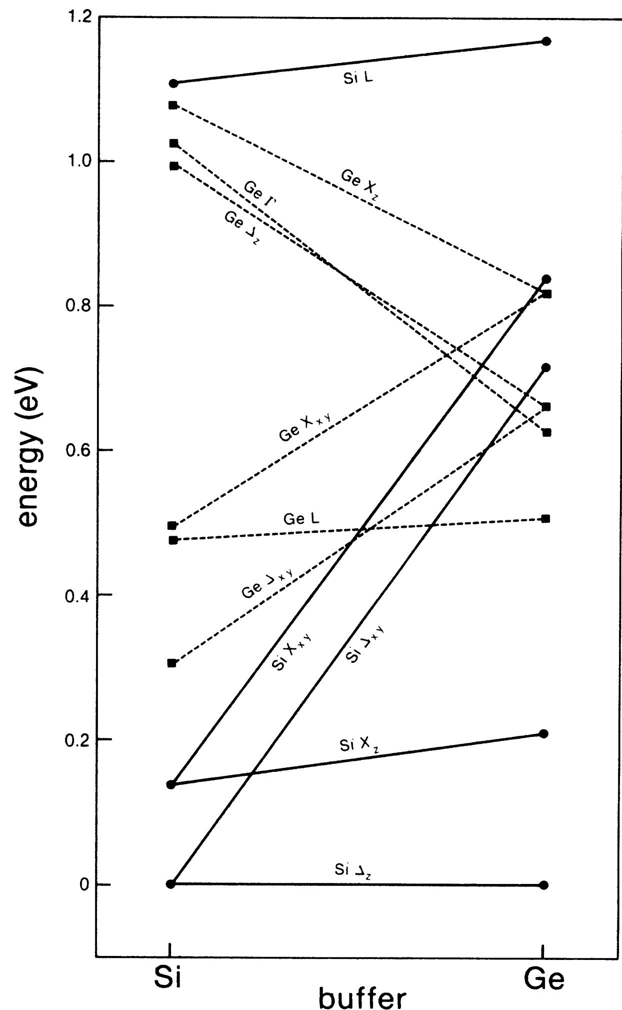

FIG. 15. Lowest bulk-crystal conduction-band levels of the Si (●) and Ge (■) superlattice layers for the case of a Si-buffered and a Ge-buffered superlattice. Corresponding levels have been joined by solid (Si) and dashed (Ge) lines. This figure has been constructed using data from Figs. 3 and 4 and band offsets given in Ref. 32. The zero of energy has been taken as the energy of the lowest conduction-band level, i.e., Si Δ_z.

the Si to the Ge buffer is caused primarily by the upward movement of the $|m_J|=\frac{1}{2}$ valence state with increasing x. For the three cases, the zone-center gap is 0.90 eV (Si buffer), 0.81 eV ($Si_{0.5}Ge_{0.5}$ buffer), and 0.64 eV (Ge buffer). Such changes in the transition energies, at least between the Si-buffered and Ge-buffered structures, should be resolvable in electroreflectance experiments. By comparing Figs. 7(a), 9, and 10, it can be seen that changing the buffer-layer composition does not substantially affect the zone-center cross-gap–transition probabilities, a reflection of the dominant role of symmetry in determining the band structure.

For the case of a Si buffer, the sixfold degeneracy of the (bulk) Δ minimum in the Si layers is not lifted, although the degeneracy of the corresponding minimum in the Ge layers is lifted (note that these bulk levels are not allowed levels within the superlattice). As the Ge concentration in the buffer layer increases, the degeneracy of the Si Δ minimum is lifted and the four $\Delta_{x,y}$ levels are raised with respect to the two Δ_z levels. This can be seen clearly in Fig. 15, in which the lowest bulk-crystal conduction-band levels of the Si and Ge layers in the superlattice have been plotted for the two extreme cases of buffer composition. The offsets used to construct Fig. 15 are those given by Van de Walle and Martin.[32] It would appear from Fig. 15 that the lowest *transverse* zone-edge-related *superlattice* state is likely to be much higher in energy than the lowest *longitudinal* zone-edge-related *superlattice* state for the case of the Ge buffer. This simple argument does of course rely on (a) the individual ultrathin layers behaving like bulk crystals, (b) crude aspects of band-folding being retained in such thin-layered structures, and (c) the band offsets predicted by Van de Walle and Martin[32] being substantially correct.

In order to check aspects (a) and (b) of this argument, superlattice states have been calculated at various points in the SBZ for a range of $Si_{1-x}Ge_x$ buffers. Energies of states $V4$–$C5$ at Γ, Δ_X, M, X, and Z are given in Table VIII for the case of a (001) Si buffer and a (001) Ge buffer. The point Δ_X corresponds to a point 82% along the [100]

TABLE VIII. Energy levels of states $V4$–$C5$ at points (of high symmetry) in the Brillouin zone of the Si/Ge (4:4) superlattice on a (001) Si substrate and on a (001) Ge substrate. In both cases, the zero of energy has been taken as the energy of state $V1$ at Γ. The wave vector labeled Δ_X corresponds to a point 82% along the [100] direction, where there is a minimum in the dispersion of state $C1$. The point labeled X corresponds to one of the two distinct points onto which host-crystal L valleys are mapped. The points labeled M and Z correspond to the edges of the minizone in the [100] and [001] directions, respectively. Energy levels which can be readily extracted from published results on the (4:4) superlattice have also been included so that *general* comparisons can be made between the results (in parentheses) of the different types of calculations, i.e., local density (LD, Ref. 16; the results for the conduction states include shifts to correct for the usual LD errors), quasiparticle (QP, Ref. 16), tight-binding (TB, Ref. 18), and effective-mass type (EM, Ref. 17; these results correspond to room temperature). The comparisons are not intended to be strict comparisons since the different calculations do not have identical inputs. Transition energies read from figures have been rounded to the nearest tenth of an eV.

Wave vector	Superlattice state $V4$	$V3$	$V2$	$V1$	$C1$	$C2$	$C3$	$C4$	$C5$	
				Si substrate						
Γ	−1.79	−0.40	−0.14	0.00	0.90	1.03	1.51	1.80	2.59	
					(1.16)	(1.27)	(1.75)	(1.94)	(2.6)	LD
		(−0.42)	(−0.1)		(1.1)	(1.24)	(1.76)	(2.0)	(2.4)	QP
			(−0.1)		(1.0)	(1.1)	(1.6)	(1.8)	(2.2)	TB
			(−0.1)		(0.97)	(1.15)	(1.59)	(−)	(2.3)	EM
Δ_X	−3.13	−3.06	−2.89	−2.85	0.79	1.44	2.21	2.56	3.43	
					(0.92)					LD
					(0.85)					QP
					(0.71)					EM
M	−3.01	−2.97	−2.80	−2.65	0.99	1.01	1.59	1.86	4.58	
				(−3)						LD
X	−1.43	−1.37	−0.99	−0.94	1.43	1.46	2.86	2.89	3.95	
				(−0.9)						LD
Z	−0.95	−0.83	−0.80	−0.74	0.83	1.05	1.83	1.91	2.39	
				Ge substrate						
Γ	−1.90	−0.25	−0.11	0.00	0.64	0.79	1.20	1.46	2.21	
			(−0.12)		(0.75)	(0.82)	(0.93)	(1.96)	(1.90)	EM
Δ_X	−2.82	−2.80	−2.55	−2.52	1.07	1.66	2.24	2.49	3.90	
M	−2.66	−2.63	−2.49	−2.37	1.25	1.27	1.65	1.83	5.01	
X	−1.20	−1.16	−1.01	−1.00	1.28	1.30	2.47	2.50	3.79	
Z	−0.96	−0.91	−0.87	−0.80	0.53	0.75	1.73	1.74	2.13	

direction, where there is a minimum in the dispersion of state *C*1; the position of this minimum is independent of the buffer composition. The point *X* corresponds to one of the two distinct points onto which host-crystal *L* valleys are mapped and the states at this point correspond to the states labeled $\bar{L}_{v,c}$ in the work of Froyen *et al.*[16] The points labeled *M* and *Z* correspond to the edges of the SBZ in the [100] and [001] directions, respectively.

It can be seen from Table VIII that state *C*1 at Δ_X lies about 0.1 eV *below* state *C*1 at Γ for the case of a Si buffer. For the case of a Ge buffer, state *C*1 at Δ_X lies 0.43 eV *above* state *C*1 at Γ. This change in relative alignment of state *C*1 at Γ and Δ_X corresponds well to the change in alignment of the bulk Δ_{xy} and Δ_z levels shown in Fig. 15. Thus, the simple argument based on strain-split bulk levels appears to work fairly well, even though the layers in the superlattice are only four monolayers thick. In the case of a Si buffer, the lowest conduction states in the superlattice-buffer system are the bulk Δ conduction states in the Si layers cladding the superlattice, whereas the uppermost valence states are the valence states in the superlattice. The situation is reversed in the case of a Ge buffer: the lowest conduction state [for the (4:4) superlattice] is the superlattice state *C*1 at *Z*, whereas the uppermost valence states are the zone-center states in the Ge layers cladding the superlattice. Changing the compositions of the layers cladding (sequence of) Si/Ge superlattices provides scope for manipulating the alignments.

Although arguments based on strain-induced shifts of bulk levels appear to hold well for understanding monotonic trends in the energy levels of the zone-edge-related superlattice states, caution must be exercised for the *L*-related states. Oscillations in the energy levels of *L*-related nonfolding states have already been described by Froyen *et al.*[16] for the (2:2)-(4:4)-(6:6) sequence of Si/Ge superlattices on (001) Si. By comparing Fig. 2(b) in the paper by Froyen *et al.*[16] with the energy levels of states *C*1 and *C*2 at *X* in Table VIII, it can be seen that both calculations predict a small splitting of the nonfolding *L*-related states in the Si/Ge (4:4) superlattice on (001) Si. As expected, this splitting is not affected much by the buffer layer (see Table VIII) since it is connected essentially with the underlying atomic repeat period for the diamond structure in the [001] direction and the matching of the superlattice layers with respect to this repeat period.

In order to make a comparison between the results of the different types of calculation [empirical pseudopotential (EP), corrected local density (LD), quasiparticle (QP), tight-binding (TB), and effective-mass-type (EM)], energy levels which can be readily extracted from published results[16–18] have also been included in Table VIII. Comparison between EP and LD squared matrix elements has already been made in Table VI. In the case of the results for the Si buffer, the different calculations identify the same states, apart from state *C*4, which is missing from the EM results, although there are discrepancies of up to 0.4 eV in the energy levels. Such discrepancies clearly pose a problem in unravelling the fairly reproducible electroreflectance spectra of Pearsall *et al.*[14] In the case of the Ge buffer, the EM predictions of People[17] differ by up to about 0.5 eV compared with the predictions of the present EP calculations. Also, the calculations of People[17] suggest that transition *V*1-*C*4 is quasidirect; this is not confirmed by the EP calculations. Corrections allowing for the overestimate of the fundamental indirect gap of Si by 0.1 eV and the underestimate of the Γ_8^v-Γ_7^c gap of Ge by 0.2 eV in the full QP calculations[61] would tend to improve agreement between the present results and the QP results for the (4:4) superlattice on (001) Si.

Returning to the question of quasidirect Si/Ge structures, it is clear that buffer layers with high concentrations of Ge must be used in order to avoid the prospect of Si/Ge superlattices being truly indirect on account of transverse zone-edge-related states or Δ conduction states in the buffer layer. However, vestiges of the bulk camel's-back structures may still be retained which result in some downward dispersion along the preferred axis. This can be seen in Fig. 16 and in Table VIII, which shows that *C*1 at *Z* is 68 and 109 meV below *C*1 at Γ for the (4:4) superlattice on (001) Si and (001) Ge, respectively. The increase in the longitudinal subband dispersion in going from a Si to a Ge buffer is connected primarily with the increase (from 137 to 214 meV; see Fig. 3) in the depth of the camel's back with increasing tetragonal distortion in the Si layers. The $\Gamma-Z$ subband width of state *C*1 is found to vary linearly with Ge concentration in the buffer layer. This downward dispersion of state *C*1 along the superlattice direction (k_z) is not present in all short-period Si/Ge superlattices. For example, in the (2:6) superlattice, state *C*1 disperses *upwards* in going out from the zone-center towards *Z* (see Fig. 17). However, the width of the miniband is only about 15–17 meV over the entire range of $Si_{1-x}Ge_x$ buffers. The (6:2) superlattices, for example, are similar to the (4:4) superlattice in that the minimum in *C*1 along the k_z direction is away from the zone center. The zone-center *V*1-*C*1 transitions in the (2:6) and (6:2) superlattices are significantly enhanced.

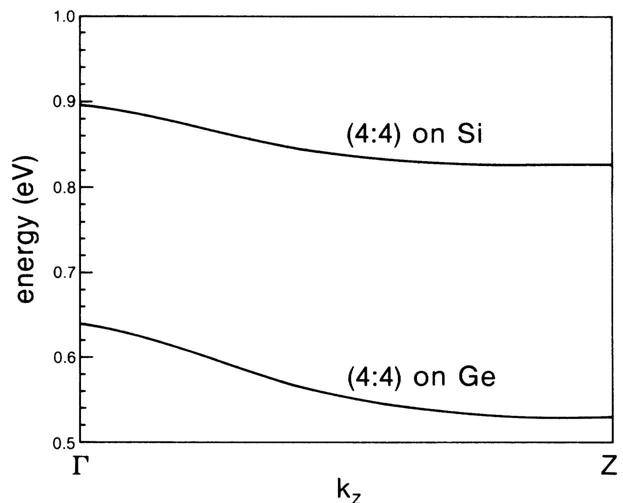

FIG. 16. Longitudinal subband dispersions of state *C*1 in the (4:4) superlattice on (001) Si and (001) Ge.

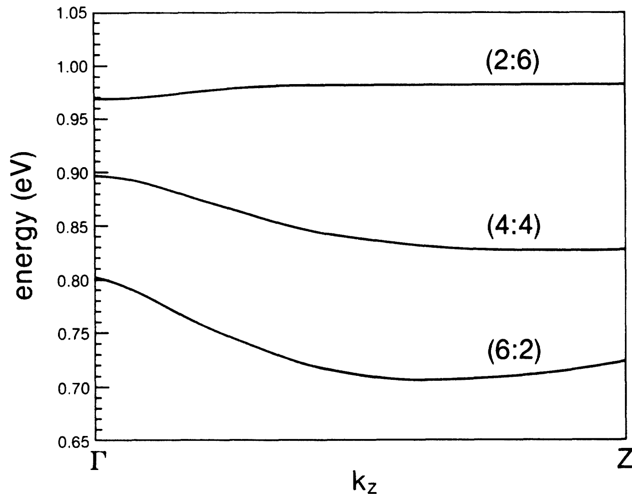

FIG. 17. Comparison between the longitudinal subband dispersions of state $C1$ in the (2:6), (4:4), and (6:2) Si/Ge superlattices on (001) Si. The zone-center energy gap decreases with increasing thickness of the Si layers.

Values of $\log_{10}$ of the modulus squared dipole matrix element for the zone-center $V1$-$C1$ transition with [110] polarization are found to be -1.7 [(2:6) superlattice on $Si_{1-x}Ge_x$] and -3.5 [(6:2) superlattice on $Si_{1-x}Ge_x$].

By calculating the energies of cross-gap transitions at X (from Table VIII), it can be seen that the lower-energy transitions for the case of a Si buffer fall into two distinct bands. The $(V1/V2)$-$(C1/C2)$ transitions span the range 2.37–2.45 eV and the $(V3/V4)$-$(C1/C2)$ transitions span the range 2.80–2.89 eV. These bands have been indicated on Figs. 7(a) at 2.3 and 2.7 eV (allowing 0.1 eV for temperature). Thus, direct allowed non-zone-center transitions account for the major structure at 2.3 eV in the electroreflectance spectrum which could not be accounted for on the basis of zone-center transitions.

In order to provide a prediction which can be used to verify the assignments given in this paper, the energies calculated for various transitions at Γ and X have been calculated as a function of buffer composition. As the Ge concentration in the buffer increases, the $(V1/V2)$-$C5$ band of zone-center transitions are predicted to overlap the lowest-energy transitions occurring at X. In terms of electroreflectance spectra for the Si/Ge (4:4) superlattice, the structure at 2.3 eV at $x=0$ is predicted to rise slightly in energy with increasing x, while the structure occurring at 2.6 eV at $x=0$ is predicted to drop and merge with the structure originating from 2.3 eV. The merger should occur for Ge concentrations in the region of 30–40 at. %. In reality, complications with line-shape analysis may make the merging structures difficult to disentangle. There should, however, be little ambiguity in detecting *converging* structures in the range $0 \le x \le 0.3$. Since the results of the quasiparticle and tight-binding calculations assign structure at 2.3 eV at $x=0$ to zone-center transitions, an increase in x would presumably be expected to give rise to *diverging* rather than *converging* structures in electroreflectance.

Marked nonlinear variations in the $(V1/V2)$-$(C1/C2)$ cross-gap transitions at X are associated with a reversal of pairs (neglecting spin) of valence states at X with changing buffer composition; this reversal is intimately connected with the hole reversal which has been demonstrated at the zone center. The transitions at X show no significant polarization dependence; the only polarization-dependent transition is the $V2$-$C5$ zone-center transition for $x \ge 0.6$. However, observation of the polarization dependence of the $V2$-$C5$ zone-center transition for the case of Ge-rich buffers may be difficult owing to overlap of transitions, which is predicted for the range $0.6 \le x \le 1.0$. The relative alignment of the zone-center and L-related states is rather independent of band offset. Electroreflectance and photocurrent experiments on (4:4) superlattices as a function of buffer composition would also provide useful information on assignments of indirect and pseudodirect transitions in the low-energy range (0.5–1.4 eV) of the spectrum since the indirect edge associated with the transverse X-related states is rapidly swept up in energy as x increases. A check on the third-derivative nature of the electroreflectance spectrum (e.g., by thermoreflectance), especially in the infrared region, would also be useful.

The question of band offsets in the Si/Ge system has been tackled using various theoretical models, although on the experimental side the picture is rather sparse. The reader is referred to the paper by Cardona and Christensen,[62] where various theoretical and experimental predictions have been compared.

In order to check the sensitivity of results presented in this paper to possible variations in the band offsets, the calculations for the Si/Ge (4:4) superlattice on Si and Ge (001) buffer layers have been repeated with offsets different from those predicted by Van de Walle and Martin.[32] In each case the Ge bulk band structure has been shifted both up and down by 0.3 eV with respect to the Si

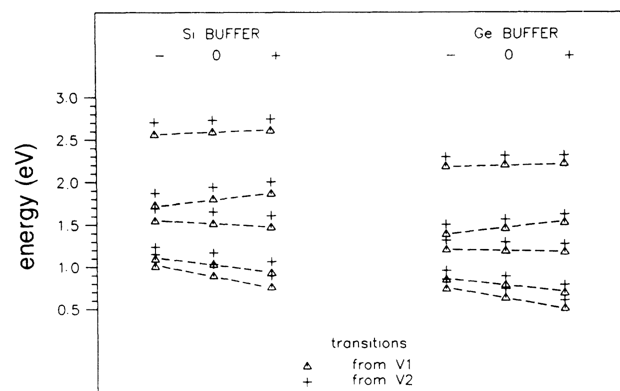

FIG. 18. Energies for transitions at the center of the superlattice Brillouin zone between the top two valence states ($V1$ and $V2$) and the bottom five conduction states ($C1$–$C5$) in the Si/Ge (4:4) superlattice on a Si buffer (left-hand side) and on a Ge buffer (right-hand side). In both cases, the column marked 0 corresponds to results obtained using the offsets given by Van de Walle and Martin (Ref. 32). The columns marked + (–) correspond to calculations in which the bulk Ge band structure has been shifted up (down) by 0.3 eV with respect to the bulk Si band structures.

bulk band structure. A shift of 0.3 eV has been chosen merely to exacerbate any changes which occur as a result of changing offsets. In Fig. 18 the transition energies for transitions at the center of the superlattice Brillouin zone between the top valence states ($V1$ and $V2$) and the bottom five conduction states ($C1-C5$) are shown for the two Si/Ge (4:4) superlattices. The case of the Si buffer is shown on the left-hand side and the case of the Ge buffer is shown on the right-hand side. In both cases, the column marked 0 corresponds to results obtained using the offsets given by Van de Walle and Martin[32] and the columns marked + (−) correspond to calculations in which the Ge band structure has been shifted up (down) by 0.3 eV with respect to the Si band structure.

It can be seen from Fig. 18 that the energies for zone-center transitions from the top of the valence band to the ground zone-center-related state $C5$ are fairly independent of offset. A similar feature has been observed in $GaAs/Al_xGa_{1-x}As$ superlattices.[22] In general, transitions to and between excited states are more sensitive to the band offset. Figure 18 shows that energies for transitions between $V1$, $V2$, and the bound conduction states ($C1-C3$) decrease with increasing valence-band offset, while energies for the transitions between $V1$, $V2$, and the resonant zone-edge-related state $C4$ increase with increasing valence-band offset. These trends can be understood qualitatively in terms of the movement of the bulk band edges and the connection between these band edges and various confined (or resonant) states. The optical matrix elements for all transitions considered in Fig. 18 show little variation within the range of offsets considered. Bearing in mind the difficulties associated with the interpretation of the electroreflectance spectra, it would be premature to attempt an assessment of the effective band offset.

VIII. COMPOSITIONAL MODULATION VERSUS ATOMIC RELAXATION

The data in Table VIII and the results concerning the hole reversal show that both the existence and distribution of tetragonal distortion play an important role in determining many of the salient features of the band structure. This is especially so in connection with the splittings and relative positions of the transverse and longitudinal zone-edge-related conduction states and in the mixing of valence states. However, it is clear from Figs. 7, 9, and 10 that the distribution of strain within the superlattice unit cell does not have a substantial effect on the magnitudes of the squared optical matrix elements for the zone-center transitions. The sizes of the matrix elements reflect the mixing of different momentum components into the superlattice wave functions. In the absence of momentum mixing, transitions from states at the top of the valence band (zone-center-derived) to states near the bottom of the conduction band (zone-edge-derived) would be dipole-forbidden. Thus, momentum mixing, leading to quasidirect transitions, has occurred as a result of the formation of the superlattice. Since the formation of the strained-layer superlattice can be viewed in terms of a process of compositional modulation followed by a process of atomic relaxation (strain accommodation), it is not obvious to what degree compositional modulation and atomic relaxation have each contributed to the enhancement of the optical matrix elements.

In order to establish the individual contributions of these processes to the enhancement of the optical transition probabilities, additional calculations have been performed in which strain has been artificially removed. For the case of the (4:4) Si/Ge superlattice on Si, this was achieved by substituting the tetragonal Ge with a cubic Ge-like material. The form factors used to generate the Ge-like band structure were −0.120, 0.050, and 0.036 a.u. The lattice constant of the Ge-like material was taken to be the same as that used for Si (see Sec. II). Bearing in mind that the tetragonal distortion splits some of the degeneracies, the Si and Ge bulk energy-band discontinuities at Γ, X, and L were arranged to be as close as possible to those used in the control calculations. These discontinuities, which are not in fact crucial, are shown in Fig. 19. $\log_{10}$ of the modulus squared optical matrix

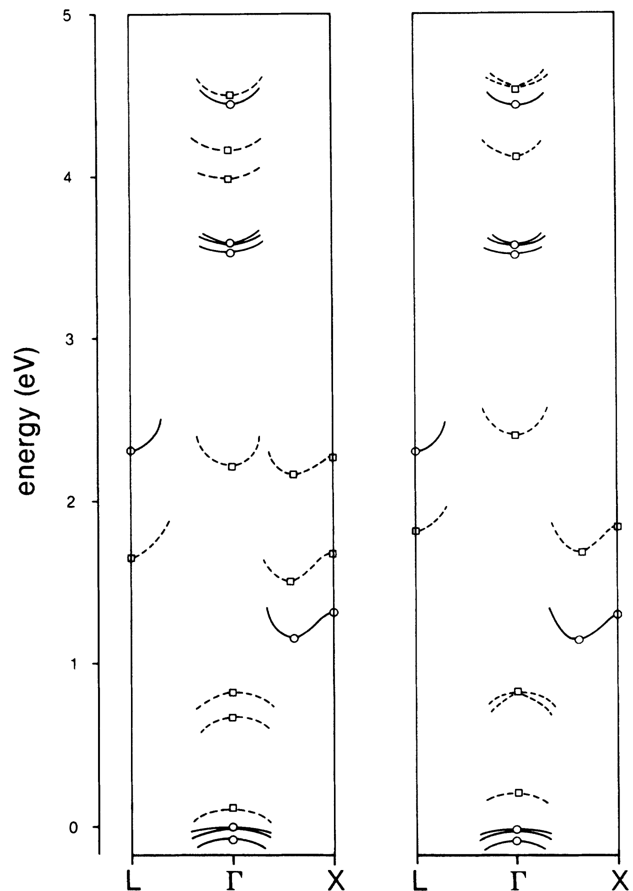

FIG. 19. Band discontinuities at Γ, X, and L used in the calculations designed to establish the individual contributions of the processes of compositional modulation and atomic relaxation to the enhancement of the optical transition probabilities (see text). The alignment of the energy levels in the diagram on the left-hand side corresponds to the case of the superlattice with layers of cubic Si alternating with layers of tetragonal Ge (see also Fig. 15). The diagram on the right-hand side corresponds to the case of the superlattice with layers of cubic Si alternating with layers of a cubic Ge-like material. In both cases the buffer layer is Si.

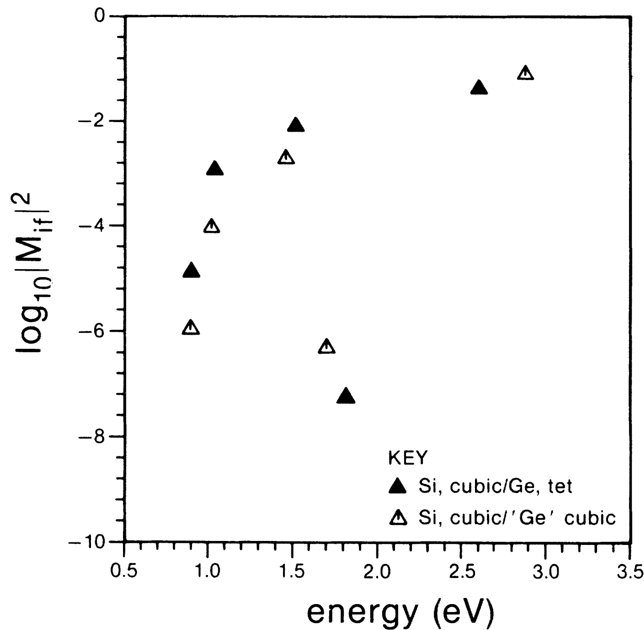

FIG. 20. Plot of $\log_{10}$ of the modulus squared of the optical matrix element against transition energy for the $V1-Ci$ $(i=1-5)$ zone-center transitions calculated for the two systems shown in Fig. 19.

elements for the zone-center transitions with [110] polarization from state $V1$ to the lowest five conduction states are shown in Fig. 20 for the cubic-tetragonal and cubic-cubic Si/Ge (4:4) superlattices on Si. The results for the cubic-tetragonal superlattice are the ones which have already been shown in Fig. 7(a). Neglecting the unimportant differences in transition energies between corresponding transitions, it can be seen from Fig. 20 that the effect of atomic relaxation on the squared matrix elements for the quasidirect transitions in an enhancement of approximately 1 order of magnitude. The already allowed direct transitions occurring at about 2.7 eV are practically unaffected by the introduction of the atomic relaxation. Thus, strain accommodation appears to produce an effect which is not insignificant only on those transitions which are, in any case, fairly weak. This can be understood qualitatively in terms of the effect of a perturbation on otherwise orthogonal functions within an overlap integral. The underlying enhancement of the quasidirect transitions and the phase factors determining the parities of the states are controlled by the compositional modulation, i.e., the layer thicknesses and the imposed reduction in dimensionality.

IX. SUMMARY

In summary, we have used results of pseudopotential calculations based on local empirical pseudopotentials with spin-orbit coupling to make a comparison with the electroreflectance data of Pearsall *et al.* for the Si/Ge (4:4) superlattice grown on a (001) Si substrate. The characters of superlattice states have been shown in terms of their real-space charge density and in terms of their origin in wave-vector space and a strain-induced crossing of $|m_J|=\frac{3}{2}$ and $\frac{1}{2}$ valence states has been demonstrated. The influence of heterointerface bond length and band offset have been examined and the individual contributions of compositional modulation and atomic relaxation to the enhancement of dipole matrix elements for cross-gap quasidirect transitions have been established. Predictions have been made for the Si/Ge (4:4) superlattice grown on the entire range of (001) $Si_{1-x}Ge_x$ $(0\leq x\leq 1)$ buffer layers. A more detailed study of critical point structure throughout the superlattice Brillouin zone which is necessary for detailed interpretation of electroreflectance spectra will be presented elsewhere.

ACKNOWLEDGMENTS

I would like to thank Philip Klipstein and Mike Burt for useful discussions and I am grateful to Mervyn Jones for his support and encouragement during the progress of this work. Acknowledgment is made to the Director of Research of British Telecommunications, plc for permission to publish this paper. I would also like to thank Dr. T. Pearsall of AT&T Bell Laboratories for granting permission to reproduce the electroreflectance spectrum in Fig. 7.

[1]E. Kasper, Surf. Sci. **174**, 630 (1986).

[2]E. Kasper and H. Daembkes, in *Proceedings of the 16th European Solid State Device Research Conference, Cambridge, 1986*, Inst. Phys. Conf. Ser. No. 82 (IOP, Bristol, 1987).

[3]J. C. Bean, in *Silicon Molecular Beam Epitaxy*, edited by E. Kasper and J. C. Bean (Chemical Rubber Co., Boca Raton, FL, in press).

[4]W. Michaelis and M. H. Pilkuhn, Phys. Status Solidi **36**, 311 (1969).

[5]U. Gnutzmann and K. Clausecker, Appl. Phys. **3**, 9 (1974).

[6]S. A. Jackson and R. People, Mater. Res. Soc. Symp. Proc. **56**, 356 (1986).

[7]H. Jorke and H. J. Herzog, in *Proceedings of the 1st International Symposium on Si Molecular Beam Epitaxy*, edited by J. C. Bean (Electrochemical Society, Pennington, NJ, 1985).

[8]G. Abstreiter, H. Brugger, T. Wolf, H. Jorke, and H. J. Herzog, Phys. Rev. Lett. **54**, 2441 (1985).

[9]R. People, J. C. Bean, and D. V. Lang, J. Vac. Sci. Technol. A **3**, 846 (1985).

[10]R. People, J. C. Bean, D. V. Lang, A. M. Sergent, H. L. Störmer, K. W. Wecht, R. T. Lynch, and K. Baldwin, Appl. Phys. Lett. **45**, 1231 (1984).

[11]I. Morrison, M. Jaros and K. B. Wong, J. Phys. C **19**, 239 (1986).

[12]I. Morrison, M. Jaros and K. B. Wong, Phys. Rev. B **35**, 9693 (1987).

[13]D. Z. Y. Ting and Y. C. Chang, J. Vac. Sci. Technol. B **4**, 1002 (1986).

[14]T. P. Pearsall, J. Bevk, L. C. Feldman, J. M. Bonar, J. P. Mannaerts, and A. Ourmazd, Phys. Rev. Lett. **58**, 729 (1987); see also J. Bevk, A. Ourmazd, L. C. Feldman, T. P. Pearsall, J. M. Bonar, B. A. Davidson, and J. P. Mannaerts, Appl. Phys.

Lett. **50**, 760 (1987); T. P. Pearsall, J. Bevk, L. C. Feldman, J. M. Bonar, J. P. Mannaerts, and A. Ourmazd, J. Vac. Sci. Technol. B **5**, 1274 (1987). Photoluminescence experiments on short-period Si/Ge superlattices grown on (110) Ge have recently been reported by K. Eberl, G. Krötz, R. Zachai, and G. Abstreiter, J. Phys. (Paris) Colloq. **48**, C5-329 (1987).

[15]The notation $m:n$ is used to denote a Si/Ge (001) superlattice in which the Si layer consists of m atomic monolayers and the Ge layer consists of n atomic monolayers, stacked in the [001] direction. The width of one atomic monolayer is approximately 1.4 Å.

[16]S. Froyen, D. M. Wood, and A. Zunger, Phys. Rev. B **36**, 4547 (1987); M. S. Hybertson and M. Schlüter, Phys. Rev. B **36**, 9683 (1987).

[17]R. People and S. A. Jackson, Phys. Rev. B **36**, 1310 (1987); R. People, in Proceedings of the Materials Research Society Spring Meeting, Anaheim, 1987, p. 299 (unpublished).

[18]L. Brey and C. Tejedor, Phys. Rev. Lett. **59**, 1022 (1987).

[19]M. Jaros and K. B. Wong, J. Phys. C **17**, L765 (1984).

[20]M. A. Gell, D. Ninno, M. Jaros, and D. C. Herbert, Phys. Rev. B **34**, 2416 (1986).

[21]M. A. Gell, D. Ninno, M. Jaros, D. J. Wolford, T. F. Keuch, and J. A. Bradley, Phys. Rev. B **35**, 1196 (1987).

[22]D. Ninno, M. A. Gell, and M. Jaros, J. Phys. C **19**, 3846 (1986).

[23]M. A. Gell and D. C. Herbert, Phys. Rev. B **35**, 9591 (1987).

[24]K. B. Wong, M. Jaros, and J. P. Hagon, Phys. Rev. B **35**, 2463 (1987).

[25]T. Isu, D. Jiang, and K. Ploog, Appl. Phys. A **43**, 75 (1987), and references therein.

[26]D. Brust, Phys. Rev. B **4**, 3497 (1971).

[27]J. C. Phillips and K. C. Pandey, Phys. Rev. Lett. **30**, 787 (1973).

[28]J. R. Chelikowsky and M. L. Cohen, Phys. Rev. Lett. **31**, 1582 (1973).

[29]J. R. Chelikowsky and M. L. Cohen, Phys. Rev. B **14**, 556 (1976).

[30]F. Bassani and D. Brust, Phys. Rev. **131**, 1524 (1963).

[31]G. Weisz, Phys. Rev. **149**, 504 (1966).

[32]C. G. Van de Walle and R. M. Martin, Phys. Rev. B **34**, 5621 (1986).

[33]Y. Hamakawa and T. Nishino, in *Optical Properties of Solids—New Developments,* edited by B. O. Seraphin (North-Holland, Amsterdam, 1976), p. 303.

[34]R. Hulthén and N. G. Nilsson, Solid State Commun. **18**, 1341 (1976).

[35]M. Neuberger, *Handbook of Electronic Materials* (Plenum, New York, 1971), Vol. 2.

[36]G. C. Osbourn, J. Appl. Phys. **53**, 1586 (1982).

[37]G. C. Osbourn, IEEE Quantum Elec. **QE-22**, 1677 (1986).

[38]F. Cerdeira, A. Pinczuk, J. C. Bean, B. Batlogg, and B. A. Wilson, Appl. Phys. Lett. **45**, 1138 (1984).

[39]J. Bevk, J. P. Mannaerts, L. C. Feldman, B. A. Davidson, and A. Ourmazd, Appl. Phys. Lett. **49**, 286 (1986).

[40]J. L. Martins and A. Zunger, Phys. Rev. Lett. **56**, 1400 (1986), and references therein.

[41]E. Kasper, H. J. Herzog, H. Daembkes, and G. Abstreiter, in Proceedings of the Materials Research Society Meeting, Boston, 1985, p. 347 (unpublished).

[42]W. A. Brantley, J. Appl. Phys. **44**, 534 (1973).

[43]L. C. Feldman, J. Bevk, B. A. Davidson, H.-J. Grossman, and J. P. Mannaerts, Phys. Rev. Lett. **59**, 664 (1987).

[44]G. L. Bir and G. E. Picus, *Symmetry and Strain-Induced Effects in Semiconductors* (Wiley, New York, 1974).

[45]A. A. Kaplyanskii, Opt. Spectrosc. (USSR) **16**, 557 (1964).

[46]E. O. Kane, Phys. Rev. **178**, 1368 (1969).

[47]R. W. Keyes, in *Solid State Physics,* edited by H. Ehrenreich, F. Seitz, and D. Turnbull (Academic, New York, 1960), Vol. 11, p. 149.

[48]F. H. Pollak, in Proceedings of the International Conference on the Physics of Semiconductors, Cambridge, 1970, p. 407 (unpublished).

[49]J. C. Hensel and G. Feher, Phys. Rev. **129**, 1041 (1963).

[50]H. Hasegawa, Phys. Rev. **129**, 1029 (1963).

[51]I. Goroff and L. Kleinman, Phys. Rev. **132**, 1080 (1963), and references therein.

[52]F. Pollak and M. Cardona, Phys. Rev. **172**, 816 (1968).

[53]I. Balslev, Phys. Rev. **143**, 636 (1966), and references therein.

[54]L. D. Laude, F. H. Pollak, and M. Cardona, Phys. Rev. B **3**, 2623 (1971).

[55]M. Chandrasekhar and F. H. Pollak, Phys. Rev. B **15**, 2127 (1977).

[56]S. L. Richardson and M. L. Cohen, Phys. Rev. B **35**, 1388 (1987), and references therein.

[57]L. Kleinman, Phys. Rev. **128**, 2614 (1962).

[58]T. C. Bonsett, M. Yamanishi, R. L. Gunshor, S. Datta, and L. A. Kolodziejski, Appl. Phys. Lett. **51**, 499 (1987).

[59]K. Nishi, K. Hirose, and T. Mizutani, Appl. Phys. Lett. **49**, 794 (1986).

[60]D. Gershoni, J. M. Vandenberg, R. A. Hamm, H. Temkin, and M. B. Panish, Phys. Rev. B **36**, 1320 (1987).

[61]M. S. Hybertson and S. G. Louie, Phys. Rev. B **34**, 5390 (1986).

[62]M. Cardona and N. E. Christensen, Phys. Rev. B **35**, 6182 (1987).